

## Journal Pre-proofs

1,4,5,6,7,8-Hexahydroquinolines and 5,6,7,8-tetrahydronaphthalenes: A new class of antitumor agents targeting the colchicine binding site of tubulin

Mennatallah A. Shaheen, Ali A. El-Emam, Nadia S. El-Gohary

PII: S0045-2068(20)30510-1  
DOI: <https://doi.org/10.1016/j.bioorg.2020.103831>  
Reference: YBIOO 103831

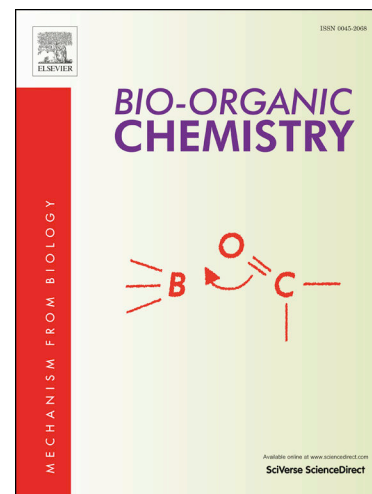
To appear in: *Bioorganic Chemistry*

Received Date: 3 March 2020  
Revised Date: 3 April 2020  
Accepted Date: 5 April 2020

Please cite this article as: M.A. Shaheen, A.A. El-Emam, N.S. El-Gohary, 1,4,5,6,7,8-Hexahydroquinolines and 5,6,7,8-tetrahydronaphthalenes: A new class of antitumor agents targeting the colchicine binding site of tubulin, *Bioorganic Chemistry* (2020), doi: <https://doi.org/10.1016/j.bioorg.2020.103831>

This is a PDF file of an article that has undergone enhancements after acceptance, such as the addition of a cover page and metadata, and formatting for readability, but it is not yet the definitive version of record. This version will undergo additional copyediting, typesetting and review before it is published in its final form, but we are providing this version to give early visibility of the article. Please note that, during the production process, errors may be discovered which could affect the content, and all legal disclaimers that apply to the journal pertain.

© 2020 Elsevier Inc. All rights reserved.



# 1,4,5,6,7,8-Hexahydroquinolines and 5,6,7,8-tetrahydronaphthalenes: A new class of antitumor agents targeting the colchicine binding site of tubulin

Mennatallah A. Shaheen<sup>a,b</sup>, Ali A. El-Emam<sup>a</sup>, Nadia S. El-Gohary<sup>a,\*</sup>

<sup>a</sup>Department of Medicinal Chemistry, Faculty of Pharmacy, Mansoura University, Mansoura 35516, Egypt

<sup>b</sup>Department of Pharmaceutical Chemistry, Faculty of Pharmacy, Horus University, New Damietta, Egypt

\*Corresponding author: [dr.nadiaelgohary@yahoo.com](mailto:dr.nadiaelgohary@yahoo.com), [nadiaelgohary2005@gmail.com](mailto:nadiaelgohary2005@gmail.com)

**ABSTRACT:** New series of 2-amino-1,4,5,6,7,8-hexahydroquinoline-3-carbonitriles **3a,b** and 2-amino-5,6,7,8-tetrahydronaphthalene-1,3-dicarbonitriles **4a-h** were synthesised and evaluated for their antitumor activity. *In vitro* antitumor evaluation of the new members against HepG2, HCT-116 and MCF-7 cancer cells showed that the tetrahydronaphthalene-1,3-dicarbonitrile **4c** has the highest potency against the three tested cancer cells ( $IC_{50} = 6.02, 8.45$  and  $6.28 \mu M$ , respectively). In addition, **4c** displayed low cytotoxicity against WI38 and WISH normal cells ( $IC_{50} = 51.78$  and  $42.36 \mu M$ , respectively), and it might be utilized as a potent and selective antitumor agent. Compound **4c** was further studied for its effect on tubulin polymerization, different phases of cell cycle, apoptosis and caspases 3/9 levels. Results revealed that analog **4c** has tubulin polymerization inhibitory effect with  $IC_{50}$  value of  $3.64 \mu M$ . Additionally, it induced significant accumulation of the tested cancer cells in G2/M phase, and induced cell death primarily *via* apoptosis. Besides, it showed evident increase in caspase-3 level in HepG2 and HCT-116, and caspase-9 level in MCF-7 cells. Further, docking study proved the exact fit of **4c** into the colchicine binding site of tubulin.

**Keywords:** Hexahydroquinolines; Tetrahydronaphthalenes; Antitumor; Tubulin polymerization inhibition; Cell cycle analysis; Apoptosis; Computational studies

## 1. Introduction

Cancer is a dreadful disease affecting human in developed as well as developing countries. It is known that one-quarter of adults' mortality is due to cancer [1]. The most common treatment options include surgery [2], chemotherapy [3] and radiotherapy [4]. Tubulin polymerization inhibition is an attractive therapy in cancer treatment. Tubulin consists of two subunits:  $\alpha$ -tubulin and  $\beta$ -tubulin which are composed of 450 and 455 amino acids, respectively [5].  $\alpha/\beta$ -Tubulin dimers could be grouped to form protofilaments in a head-to-tail fashion [6]. Thirteen protofilaments interact side to side forming cylinder which is polar and hollow, and they are called microtubules (MTs). Cell division, cell migration and intracellular transport were regulated by MTs [7]. Therefore, disruption of the function of MTs will lead to mitotic arrest and tumor cell death by apoptosis.

### 1.1. Rational drug design

One of the most fundamental pockets in tubulin is the colchicine binding site that has been focused on in the design of tubulin polymerization inhibitors. Nguyen and coworkers [8] selected fifteen colchicine binding site inhibitors (CBSIs) based on their harmonious topology and binding modes as well as their ability to occupy the same chemical space. They chose tubulin-DAMA-colchicine crystal structure as a template for their study, and results revealed that CBSIs interact with tubulin primarily through different hydrogen bonding interactions. They concluded that the fifteen CBSIs showed hydrogen bonding interactions with thiol of Cys  $\beta$ 239. Out of the fifteen CBSIs, eleven members formed hydrogen bonding interactions with Val  $\alpha$ 179 nitrogen atom. Additionally, hydrogen bonds formed with the nitrogen atoms of Asp  $\beta$ 249, Ala  $\beta$ 248 and Leu  $\beta$ 250 were detected in eight members, whereas one hydrogen bonding interaction was formed with the oxygen atom of Thr  $\alpha$ 179 in four members. Accordingly, they constructed a common pharmacophore model based on the binding modes of these compounds. The consistent structural features and repeated ligand-tubulin interactions were the basis for the pharmacophoric points of CBSIs. Therefore, the different classes of CBSIs were suggested based on the seven-point pharmacophore comprised of one hydrogen bond donor (D1), three hydrogen bond acceptors (A1, A2 and A3), one planar group (R1) and two hydrophobic

centers (H1 and H2) (Fig. 1). Based on these formerly reported facts, we can conclude that compounds exhibiting these seven pharmacophoric features will be considered as promising tubulin polymerization inhibitors. Taking colchicine as a lead for synthesis of the new members, its structure consists of three rings: ring A, ring B (linker) and ring C. Structure–activity relationship study revealed that rings A and C of colchicine are prerequisites for its high binding affinity to colchicine binding site of tubulin. The changes of the linker region influence the cytotoxic activity of the most reported CBSIs [8]. Fig. 2 illustrates the pharmacophoric points of colchicine as a lead for synthesis of new CBSIs.

Lots of CBSIs of natural and synthetic origins have been developed, and they are structurally in common [9–11]. Literature survey proved that naphthalene derivatives **A–D** have promising antitumor activity through tubulin polymerization inhibition (Fig. 3) [12–17]. Also, quinoline derivatives **E–G** were proved to have excellent antitumor activity through tubulin polymerization inhibition (Fig. 3) [18–23]. Further, the 4,6-diarylpyridine-3-carbonitrile **H** [24], and 7-aryl-5-indolyimidazo[1,2-*a*]pyridine-8-carbonitriles **I** [25] and **J** [26] were reported as antitumors and CBSIs (Fig. 4). Recently, 4-aryl-4*H*-chromene derivatives **K** [27] and **L, M** [28] were identified as anticancer agents that exert their potency *via* tubulin polymerization inhibition (Fig. 4). In addition, the 4-aryl-4*H*-chromenes were reported as apoptosis inducers through elevation of caspases levels [29]. Crolibulin (Figs. 4 and 5) is a 4-aryl-4*H*-chromene derivative, and it is a promising antitumor agent that inhibits tubulin polymerization into MTs *via* binding to the colchicine binding site of tubulin, leading to cell cycle arrest in G2/M phase, apoptosis and suppression of tumor cell proliferation [27]. Structure-activity relationship study of 4-aryl-4*H*-chromenes revealed that presence of cyano group at 3-position played a significant role on their antitumor activity, and introduction of a phenyl moiety at 4-position considerably improved the potency [27–29]. In the current research, 4*H*-chromene ring in crolibulin was replaced by hexahydroquinoline or tetrahydronaphthalene, and the cyano group at 3-position as well as the aromatic ring at 4-position were retained in order to prepare a new series of 4-arylhexahydroquinolines **3a,b** (Fig. 5); in addition, an attempt to improve the binding interaction with the target protein was achieved by the introduction of an extra cyano group at 1-position to prepare a new series of 4-aryltetrahydronaphthalene-1,3-dicarbonitriles **4a-h** with expected antitumor and tubulin polymerization inhibitory activities (Fig. 5).

## 2. Results and discussion

### 2.1. Chemistry

As described in [Scheme 1](#), the arylidenemalononitriles **1a,b** and **2a-h** [30-36] were prepared *via* condensation of the appropriate aromatic aldehydes with malononitrile in ethanol [36]. The arylidenemalononitriles **1a,b** were allowed to react with cyclohexanone and excess ammonium acetate *via* heating in ethanol to yield the expected 2-amino-4-aryl-1,4,5,6,7,8-hexahydroquinoline-3-carbonitriles **3a** and **3b** in 85 and 72% yields, respectively, this reaction was previously described by El-Ashmawy *et al.* [37]. The structures of the hexahydroquinoline-3-carbonitrile derivatives **3a,b** were confirmed based on IR,  $^1\text{H}$  NMR,  $^{13}\text{C}$  NMR and Electrospray Ionization mass spectral (ESI-MS) data.  $^1\text{H}$  NMR spectra of both compounds showed characteristic singlets at  $\delta$  5.10 and 5.04 ppm corresponding to  $\text{C}_4\text{-H}$ , and  $^{13}\text{C}$  NMR spectra showed signals at  $\delta$  33.2 and 32.7 ppm corresponding to C-4. Additionally, ESI-MS spectra of compounds **3a,b** were in agreement with their exact mass values, for example, mass spectrum of **3a** showed ( $\text{M}^++\text{H}$ ) peak at 320.0 corresponding to its exact mass 319.06. Unlike the reaction of arylidenemalononitriles **1a,b** with cyclohexanone and ammonium acetate, the reaction of arylidenemalononitriles **2a-h** with cyclohexanone and ammonium acetate under the same reaction conditions did not yield the expected hexahydroquinoline-3-carbonitrile analogs, and instead they yielded the unexpected 2-amino-4-aryl-5,6,7,8-tetrahydronaphthalene-1,3-dicarbonitrile derivatives **4a-h** in 66-90% yields. A similar observation was previously reported by Al-Youbi *et al.* [38] and Asiri *et al.* [39,40]. The possible mechanism of the formation of 5,6,7,8-tetrahydronaphthalene-1,3-dicarbonitriles **4a-h** is described in [Scheme 2](#) following the previously reported mechanism [41].

The structural assignments of compounds **4a-h** were relied on their  $^1\text{H}$  NMR,  $^{13}\text{C}$  NMR and ESI-MS spectral data.  $^1\text{H}$  NMR spectra revealed the absence of the singlet characteristic for  $\text{C}_4\text{-H}$  in all derivatives. In addition, ESI-MS spectra of compounds **4a-h** were in agreement with their exact mass values, for example, mass spectrum of **4d** showed ( $\text{M}^++\text{H}$ ) peak at 310.2 corresponding to its exact mass 309.11. The structures of the tetrahydronaphthalene-1,3-dicarbonitrile derivatives **4a-h** were further confirmed by single crystal X-ray crystallography of compounds **4b** ([Fig. 6A](#)) and **4d** ([Fig. 6B](#)).

## 2.2. Biology

### 2.2.1. Cytotoxicity testing

#### 2.2.1.1. *In vitro* antitumor testing against cancer cells

MTT assay was followed to evaluate the antitumor activity of the new derivatives **3a,b** and **4a-h** against hepatocellular carcinoma (HepG2), colorectal carcinoma (HCT-116) and breast carcinoma (MCF-7) [42,43]. Concentrations of compounds that induce 50% inhibition of cell viability ( $IC_{50}$ ,  $\mu\text{M}$ ) were determined and compared to doxorubicin and colchicine as reference agents (Table 1).

Results showed that **4c** is the most potent member against all chosen cancer cells ( $IC_{50}$  = 6.02-8.45  $\mu\text{M}$ ). On the other hand, **4b** exhibited strong activity against MCF-7 cancer cells ( $IC_{50}$  = 10.15  $\mu\text{M}$ ), and moderate activity against HepG2 and HCT-116 cells ( $IC_{50}$  = 26.80 and 12.40  $\mu\text{M}$ , respectively). Further, **4a** and **4g** were proved to have moderate activity against all tested cell lines ( $IC_{50}$  = 11.39-30.93  $\mu\text{M}$ ). On the opposite side, **3b** was proved to be moderately active against HepG2 and HCT-116 cell lines ( $IC_{50}$  = 32.59 and 36.56  $\mu\text{M}$ , respectively). The remaining members displayed low or no activity against the three chosen cancer cells.

#### *Structure-activity relationship*

Concerning the hexahydroquinolines **3a,b**, presence of 2,4-difluorophenyl moiety at 4-position of hexahydroquinoline ring resulted in moderate activity against HepG2 and HCT-116 cells, and weak activity against MCF-7 cells (compound **3b**). Replacement of 2,4-difluorophenyl moiety in **3b** with 2,3-dichlorophenyl counterpart resulted in weak activity against the three tested cancer cells (compound **3a**).

With respect to the activity of tetrahydronaphthalenes **4a-h**, the 4-(2-chloro-6-fluorophenyl)tetrahydronaphthalene derivative **4c** showed the highest activity against the three chosen cancer cells. Replacement of 2-chloro-6-fluorophenyl moiety in **4c** with 2,6-dichlorophenyl counterpart gave compound **4a** with moderate activity against the three cell lines, whereas its replacement with 3,4-dichlorophenyl moiety gave compound **4b** with strong

activity against MCF-7 cells, and moderate activity against HepG2 and HCT-116 cells. In addition, replacement of 2-chloro-6-fluorophenyl moiety in **4c** with 2,6-difluorophenyl counterpart resulted in weak or abolished activity against the selected cancer cells (derivative **4d**), and this might be attributed to the additional chlorine-binding interaction of **4c** with target protein (chlorine is a good halogen-bond donor [44]), whereas fluorine in **4d** is generally considered to be a poor halogen-bond donor [44], and hence **4d** is expected to show no halogen-binding interaction with the target protein. Likewise, replacing 2-chloro-6-fluorophenyl moiety in **4c** with biphenyl resulted in weak activity against the selected cancer cells (derivative **4e**). Further, presence of naphthalen-2-yl moiety at 4-position of tetrahydronaphthalene ring resulted in moderate activity against the three tested cancer cells (compound **4g**). Replacing naphthalen-2-yl in **4g** with anthracen-9-yl led to decreased activity against the three tested cancer cells (compound **4h**), whereas its replacement with [1,3]benzodioxol-4-yl resulted in weak activity against HepG2, and abolished activity against the selected colorectal and breast cancer cells (compound **4f** versus **4g**). Comparing the activity of **3a,b** and **4a-h**, it is obvious that compounds **4a-c** and **4g,h** are more potent antitumor agents than **3a,b**, and this might be attributed to the presence of an extra cyano group at 1-position of tetrahydronaphthalene nucleus in **4a-c** and **4g,h** that was proved to be involved in additional hydrogen bonding interaction with the colchicine binding site of tubulin.

#### 2.2.1.2. *In vitro* cytotoxicity testing of **4c** against normal cells

Cytotoxicity of **4c** against WI38 lung fibroblast and WISH amnion epithelial normal cells was evaluated following MTT assay [42,43].  $IC_{50}$  values ( $\mu\text{M}$ ) were determined, and results are compared to doxorubicin. Compound **4c** showed lower cytotoxicity toward WI38 and WISH normal cells ( $IC_{50} = 51.78$  and  $42.36 \mu\text{M}$ , respectively) than doxorubicin ( $IC_{50} = 6.72$  and  $3.80 \mu\text{M}$ , respectively), and it was evidenced to be safe against the tested normal cells at their cytotoxic concentrations against the tested cancer cells.

## 2.2.2. Mechanistic studies

### 2.2.2.1. Screening of tubulin polymerization inhibitory activity

Crolibulin was proved to exert its antitumor activity through inhibition of tubulin polymerization [27]. Due to structural similarity between the most active antitumor member in the current research (compound **4c**) and crolibulin (Fig. 5), and as an attempt to explore the possible mode of action of **4c**, its *in vitro* tubulin polymerization inhibitory activity was assessed [45,46]. Results indicated that **4c** is a good tubulin polymerization inhibitor ( $IC_{50} = 3.64 \mu\text{M}$ ) in comparison to colchicine ( $IC_{50} = 1.28 \mu\text{M}$ ) (Fig. 7). In addition, **4c** induced % tubulin polymerization inhibitory activity of 54.11% at concentration of  $10 \mu\text{M}$  in comparison to colchicine with % inhibition value of 61.25% at same concentration.

### 2.2.2.2. Flow cytometry analysis of cell cycle

The structural similarities between the most active antitumor compound **4c** and crolibulin, as well as the promising inhibition of tubulin dynamics led us to hypothesize that it exerts its antiproliferative properties through inducing G2/M arrest in cancer cells similarly to tubulin polymerization inhibitors that were reported to induce G2/M arrest in cancer cells [46,47]. Therefore, compound **4c** was studied for its ability to arrest cell cycle adopting the propidium iodide (PI) flow cytometry assay kit [48-52].

Compound **4c** was incubated with HepG2, HCT-116 and MCF-7 cancer cells for 24 h, then changes within the cell cycle were observed. The cell cycle histograms of the three cancer cells treated with compound **4c** (at  $IC_{50}$  of the corresponding cell line) are illustrated in Fig. 8. The observations of cell cycle arrest induced by **4c** in the three cancer cell lines are shown in Fig. 8 and compared to that of the untreated cells. Regarding the results of cell cycle arrest in HepG2, compound **4c** increased the percentage of cells in pre-G1 phase (from 1.29% to 24.03%) and G2/M phase (from 5.62% to 35.72%), and decreased the percentage of cells in S phase (from 36.12% to 24.82%) and Go/G1 phase (from 58.26% to 39.46%) (Fig. 8). Referring to the results of cell cycle arrest in HCT-116, compound **4c** increased the percentage of cells in pre-G1 phase from (2.19% to 26.59%) and G2/M phase (from 21.20% to 45.91%), and decreased the percentage of cells in S phase (from 31.52% to 25.66%) and Go/G1 phase (from 47.28% to

28.43%) (Fig. 8). Regarding the results of cell cycle arrest in MCF-7, compound **4c** increased the percentage of cells in pre-G1 phase (from 1.85% to 22.42%), G2/M phase (from 16.69% to 35.77%) and S phase (from 29.49% to 31.42%), and decreased the percentage of cells in Go/G1 phase (from 53.82% to 32.81%) (Fig. 8). From the above results, we can conclude that **4c** demonstrated significant increase in the cell population of the three tested cancer cell lines in G2/M phase, and induced cellular apoptosis in pre-G1 phase (Fig. 8), and accordingly stopped the mitotic cycle. This action came in agreement with the well known fact that tubulin polymerization inhibitors prevent the cancer cells from beginning mitosis [46,47].

#### 2.2.2.3. Cell apoptosis

Cancer is one of the diseases where too little apoptosis occurs, resulting in development of malignant cells that will not die. Apoptosis is well-known as a popular target in cancer treatment [53]. The mechanism of apoptosis is complex and involves many pathways [53]. Several studies evidenced that tubulin polymerization inhibitors are capable of inducing cellular apoptosis [27,46,47]. Therefore, compound **4c** was studied for its capability to induce apoptosis in the three cancer cell lines applying the annexin V/PI double staining flow cytometry assay [48-52]. The dot plot flow cytometry assay data of the cells pigmented with PI and annexin fluorescein isothiocyanate (V-FITC) are shown in Fig. 9. The annexin V/PI double staining disclosed that after 24 h of exposure, compound **4c** (at  $IC_{50}$  of the corresponding cell line) induced early and late apoptosis in the three cancer cell lines in comparison to the untreated cells. The proportion of total apoptosis in HCT-116 cells treated with compound **4c** was more than that of MCF-7 and HepG2 cells (Fig. 9). On contrary, compound **4c** induced weak necrosis in the three treated cancer cells (Fig. 9) confirming that cell death induced by compound **4c** occurs primarily through apoptosis.

#### 2.2.2.4. Caspases 3/9 activation assay

Caspases represent a family of cysteine proteases that are present in the cytosol, and they are correlated with cell apoptosis through the mitochondrial pathway [54]. The most common members in the caspases family are caspases 3/9, the activation of which triggers cell apoptosis [55]. Therefore, drugs that elevate the levels of caspases are considered to be potent apoptosis

inducers [56]. Caspase-3 is expressed in HepG2 and HCT-116 cell lines [57,58], whereas MCF-7 cancer cells do not express this type of caspase [59,60], and instead they express caspase-9 [61,62]. Consequently, compound **4c** (at concentration of 10  $\mu\text{M}$ ) was assessed for its ability to elevate the levels of caspase-3 in HepG2 and HCT-116 [63], and caspase-9 in MCF-7 [63]. Results (Fig. 10A) revealed that **4c** increased the level of caspase-3 in HepG2 and HCT-116 by about 10 and 5 folds, respectively compared to the corresponding untreated cells. On the other hand, **4c** increased the level of caspase-9 in MCF-7 cancer cells by about 8 folds compared to the corresponding untreated cells (Fig. 10B).

### 3. Computational aided studies

#### 3.3. Analysis of 4c-tubulin interaction

Docking study was applied to identify the possible binding interactions between the active candidate **4c** and tubulin, and hence to explore the key structural features affecting its tubulin polymerization inhibitory activity. Docking study will provide some insights into the additional structural alterations and development of new more potent and selective tubulin polymerization inhibitors. In the present research, a molecular modeling study relied on tubulin-(DAMA-colchicine) complex crystal structure (PDB code: 4O2B) [64] was executed applying “molecular operating environment (MOE) version 2019.01” Chemical Computing Group Inc. software [65] in order to attain an idea about the binding mode of the efficacious member **4c** to the colchicine binding site of tubulin which is present at the interface between the  $\alpha$  and  $\beta$  chains of tubulin.

Primarily, the molecular docking setup was validated by implementing the re-docking of colchicine close to the colchicine binding site. The re-docking validation step reproduced the experimental binding mode of the co-crystallized ligand quite efficiently indicating the suitability of the used setup for the intended docking study, and this is confirmed by the small root-mean-square deviation (RMSD) of 0.66 Å (<2 Å) between the docked pose and the co-crystallized ligand, and by the capability of the docking poses to reproduce the key interactions achieved by the co-crystallized ligand with the hot spot amino acid (Val181) in the active site (Fig. 11).

Analysis of docking results (Fig. 12) revealed that compound **4c** showed a consistent binding mode (docking energy score ( $\Delta G$ ) = -6.05 kcal/mol) like that of the co-crystallized ligand (DAMA-colchicine) (docking energy score ( $\Delta G$ ) = -8.09 kcal/mol), including two hydrogen bonding interactions of the cyano group in compound **4c** with Val181 and Ala180 residues of  $\alpha$ -tubulin, and one hydrogen bonding interaction of amino group in **4c** with Met259 of  $\beta$ -tubulin. Furthermore, **4c** displayed an extra binding interaction with  $\beta$ -tubulin through the electrophilic chlorine atom in **4c** with nucleophilic oxygen atom in Lys352 (Fig. 12).

Also, superimposition of the co-crystallized colchicine ligand and the docking pose of compound **4c** at the colchicine binding site showed the overlap of the aryl rings in **4c** with rings A and C of colchicine (Fig. 13). To further elucidate the structural similarity between compound **4c** and colchicine, flexible alignment was carried out and they showed high structural similarity (Fig. 14). On the other hand, docking study revealed that the weak antitumor activity of **4d** (carrying 2,6-difluorophenyl substituent at 4-position of tetrahydronaphthalene nucleus) compared to the potent analog **4c** (carrying 2-chloro-6-fluorophenyl substituent at 4-position of tetrahydronaphthalene nucleus) might be due to the absence of halogen-bonding interaction in **4d** (Fig. 15), since fluorine atom in **4d** is considered to be a poor halogen-bond donor [44], whereas chlorine atom in **4c** is considered to be a good halogen-bond donor [44]. The obtained results proved that **4c** can bind to colchicine binding site to a good extent, and it occupied the active site similarly to the co-crystallized colchicine (Fig. 13), and hence it might exert its antitumor activity *via* tubulin polymerization inhibition.

## 4. Conclusion

Results of antitumor assay assured that compound **4c** is the most active member against HepG2, HCT-116 and MCF-7 cancer cells ( $IC_{50}$  = 6.02, 8.45 and 6.28  $\mu$ M, respectively). Furthermore, it displayed low cytotoxicity against WI38 and WISH normal cells ( $IC_{50}$  = 51.78 and 42.36  $\mu$ M, respectively), and it might be utilized as a potent and selective antitumor agent. Results of tubulin polymerization inhibition assay proved that **4c** has good tubulin polymerization inhibitory activity. Cell cycle analysis demonstrated that **4c** induces cell cycle arrest in G2/M phase in the three cancer cell lines, and this result comes in agreement with the fact that tubulin polymerization inhibitors strongly arrest cell cycle in G2/M phase. In addition,

the death of cancer cells induced by **4c** was proved to occur primarily through apoptosis. Referring to results of caspases 3/9 assay, compound **4c** elevated caspase-3 (in HepG2 and HCT-116 cells) and caspase-9 levels (in MCF-7 cells) confirming that apoptosis might have been occurred *via* increasing caspases 3/9 levels. Further, docking study proved the exact fit of **4c** into the colchicine binding site of tubulin. The previously presented results proved that rational design of the new hexahydroquinolines and tetrahydronaphthalenes with expected antitumor and tubulin polymerization inhibitory activities was adequate, and the most active member in the current study (compound **4c**) will be subjected to extra structural modifications in order to obtain new members with higher potency.

## 5. Experimental

### 5.1. Chemistry

Melting points (°C) were determined by Stuart melting point (SMP30) apparatus. IR spectral analysis were carried out in KBr disc on Unicam SP 1000 IR spectrometer ( $\nu$  in  $\text{cm}^{-1}$ ).  $^1\text{H}$  and  $^{13}\text{C}$  NMR spectral analysis were carried out on Bruker Avance III HD FT-high resolution (400 MHz), (500 MHz) and (700 MHz). Chemical shifts are expressed in  $\delta$  ppm with reference to tetramethylsilane. Electrospray Ionization mass spectra (ESI-MS) were recorded on Agilent 6410 Triple Quad tandem mass spectrometer at 4.0 and 3.5 kV for positive and negative ions, respectively. Elemental analyses (% C, H, N) were determined, and they were found to be in agreement with the expected structures within  $\pm 0.4\%$  of the calculated values. Reaction times were controlled by TLC plates (Silica gel 60 F254, E. Merck), and spots were visualized by UV. Hexane/ethyl acetate (9:1) was used for elution. The arylidenemalononitriles **1a,b** and **2a-h** were synthesized following the reported procedure [36].

#### 5.1.1. Synthesis of 2-amino-4-(substituted phenyl)-1,4,5,6,7,8-hexahydroquinoline-3-carbonitriles **3a,b** and 2-amino-4-aryl-5,6,7,8-tetrahydronaphthalene-1,3-dicarbonitriles **4a-h**

A mixture of the appropriate arylidenemalononitrile **1a,b** or **2a-h** (0.005 mol), cyclohexanone (0.49 g, 0.005 mol) and ammonium acetate (0.77 g, 0.01 mol, excess) was

refluxed in absolute ethanol for 6-12 h. The precipitated solid was filtered and crystallized from ethanol to produce compounds **3a,b** and **4a-h**, respectively.

*5.1.1.1. 2-Amino-4-(2,3-dichlorophenyl)-1,4,5,6,7,8-hexahydroquinoline-3-carbonitrile (3a)*

Yield 85%, m.p. 285-287 °C. IR: 3443, 3300 (NH<sub>2</sub>); 3195 (NH); 2213 (C≡N). <sup>1</sup>H NMR (500 MHz, CDCl<sub>3</sub>): δ 1.68–1.74 (m, 2H, CH<sub>2</sub>), 1.85 (t, *J* = 6.0 Hz, 2H, CH<sub>2</sub>), 2.24-2.30 (m, 2H, CH<sub>2</sub>), 2.86-2.91 (m, 2H, CH<sub>2</sub>), 5.10 (s, 1H, C<sub>4</sub>-H), 5.49 (s, 1H, NH, D<sub>2</sub>O-exchang.), 7.03-7.10 (dd, *J* = 2.0, 1.5 Hz, 1H, Ar-H), 7.35 (t, *J* = 8 Hz, 1H, Ar-H), 7.57-7.59 (m, 1H, Ar-H). <sup>13</sup>C NMR: δ 21.7, 22.2, 25.6, 29.5, 33.3, 89.5, 114.8, 127.8, 128.0, 129.0, 130.7, 131.1, 134.0, 147.4, 161.0, 162.0. ESI-MS, *m/z*: 320.0 [M+H]<sup>+</sup>. Anal. Calcd. (Found) for C<sub>16</sub>H<sub>15</sub>Cl<sub>2</sub>N<sub>3</sub> (319.06): C, 60.01 (60.37); H, 4.72 (4.43); N, 13.12 (13.46).

*5.1.1.2. 2-Amino-4-(2,4-difluorophenyl)-1,4,5,6,7,8-hexahydroquinoline-3-carbonitrile (3b)*

Yield 72%, m.p. 148-149 °C. IR: 3421, 3354 (NH<sub>2</sub>); 3307 (NH); 2216 (C≡N). <sup>1</sup>H NMR (500 MHz, CDCl<sub>3</sub>): δ 1.65-1.75 (m, 2H, CH<sub>2</sub>), 1.80-1.86 (m, 2H, CH<sub>2</sub>), 2.20-2.41 (m, 2H, CH<sub>2</sub>), 2.80-2.98 (m, 2H, CH<sub>2</sub>), 5.04 (s, 1H, C<sub>4</sub>-H), 5.29 (s, 1H, NH, D<sub>2</sub>O-exchang.), 6.94-7.03 (m, 2H, Ar-H), 7.17-7.23 (m, 1H, Ar-H). <sup>13</sup>C NMR: δ 22.2, 22.4, 25.6, 29.5, 32.7, 90.9, 104.5-104.9 (m), 112.1 (d, *J* = 21.5 Hz), 115.1 (d, *J* = 16.3 Hz), 115.7, 119.6-119.8 (dd, *J* = 3.7, 3.6 Hz), 127.2, 131.2-131.6 (m), 158.3 (t, *J* = 12.2 Hz), 160.3 (t, *J* = 11.9 Hz), 162.8 (t, *J* = 13.3 Hz). ESI-MS, *m/z*: 288.1 [M+H]<sup>+</sup>. Anal. Calcd. (Found) for C<sub>16</sub>H<sub>15</sub>F<sub>2</sub>N<sub>3</sub> (287.12): C, 66.89 (66.52); H, 5.26 (5.59); N, 14.63 (14.31).

*5.1.1.3. 2-Amino-4-(2,6-dichlorophenyl)-5,6,7,8-tetrahydronaphthalene-1,3-dicarbonitrile (4a)*

Yield 83%, m.p. 220-222 °C. IR: 3419, 3304 (NH<sub>2</sub>); 2212 (2C≡N). <sup>1</sup>H NMR (400 MHz, CDCl<sub>3</sub>): δ 1.71-1.74 (m, 2H, CH<sub>2</sub>), 1.84-1.88 (m, 2H, CH<sub>2</sub>), 2.28-2.38 (m, 2H, CH<sub>2</sub>), 2.84 (t, *J* = 8.1 Hz, 2H, CH<sub>2</sub>), 5.10 (s, 2H, NH<sub>2</sub>, D<sub>2</sub>O-exchang.), 7.12-7.14 (dd, *J* = 2.0, 2.0 Hz, 1H, Ar-H), 7.38 (d, *J* = 2.0 Hz, 1H, Ar-H), 7.58 (d, *J* = 8.2 Hz, 1H, Ar-H). <sup>13</sup>C NMR: δ 22.4, 22.7, 26.4, 33.3, 89.5, 92.1, 116.2, 120.6, 127.6, 130.1, 130.9, 133.4, 135.9, 151.7, 157.0, 162.1. ESI-MS, *m/z*: 342.1 [M+H]<sup>+</sup>. Anal. Calcd. (Found) for C<sub>18</sub>H<sub>13</sub>Cl<sub>2</sub>N<sub>3</sub> (341.05): C, 63.17 (63.51); H, 3.83 (3.49); N, 12.28 (12.51).

*5.1.1.4. 2-Amino-4-(3,4-dichlorophenyl)-5,6,7,8-tetrahydronaphthalene-1,3-dicarbonitrile (4b)*

Yield 90%, m.p. 233-235 °C. IR: 3420, 3304 (NH<sub>2</sub>); 2212 (2C≡N). <sup>1</sup>H NMR (400 MHz, CDCl<sub>3</sub>): δ 1.67-1.75 (m, 2H, CH<sub>2</sub>), 1.83-1.89 (m, 2H, CH<sub>2</sub>), 2.28-2.39 (m, 2H, CH<sub>2</sub>), 2.82-2.85 (m, 2H,

CH<sub>2</sub>), 5.20 (s, 2H, NH<sub>2</sub>, D<sub>2</sub>O-exchang.), 7.12-7.14 (dd,  $J = 2.8, 2.8$  Hz, 1H, Ar-H), 7.38 (d,  $J = 2.8$  Hz, 1H, Ar-H), 7.59 (d,  $J = 8.0$  Hz, 1H, Ar-H). <sup>13</sup>C NMR:  $\delta$  22.4, 22.7, 26.4, 33.3, 89.5, 91.5, 116.2, 117.3, 120.6, 127.6, 130.1, 130.9, 133.1, 133.4, 135.9, 151.7, 157.0, 162.1. ESI-MS,  $m/z$ : **342.1** [M+H]<sup>+</sup>. Anal. Calcd. (Found) for C<sub>18</sub>H<sub>13</sub>Cl<sub>2</sub>N<sub>3</sub> (**341.05**): C, 63.17 (63.42); H, 3.83 (3.51); N, 12.28 (12.59).

*5.1.1.5. 2-Amino-4-(2-chloro-6-fluorophenyl)-5,6,7,8-tetrahydronaphthalene-1,3-dicarbonitrile (4c)*

Yield 66%, m.p. 120-122 °C. IR: 3448, 3378 (NH<sub>2</sub>); 2215, 2169 (2C≡N). <sup>1</sup>H NMR (400 MHz, CDCl<sub>3</sub>):  $\delta$  1.70-1.76 (m, 2H, CH<sub>2</sub>), 1.86-1.90 (m, 2H, CH<sub>2</sub>), 2.25-2.29 (m, 2H, CH<sub>2</sub>), 2.88 (t,  $J = 6.4$  Hz, 2H, CH<sub>2</sub>), 5.33 (s, 2H, NH<sub>2</sub>, D<sub>2</sub>O-exchang.), 7.14-7.18 (m, 1H, Ar-H), 7.36-7.45 (m, 2H, Ar-H). <sup>13</sup>C NMR:  $\delta$  21.8, 22.1, 25.1, 31.7, 92.1, 98.0, 114.5, 114.7, 114.9, 122.7, 125.9 (d,  $J = 3.5$  Hz), 131.7 (d,  $J = 9.2$  Hz), 133.3 (d,  $J = 4.1$  Hz), 148.6, 155.8, 157.7, 159.3, 160.2. ESI-MS,  $m/z$ : **324.5** [M-H]<sup>+</sup>. Anal. Calcd. (Found) for C<sub>18</sub>H<sub>13</sub>ClFN<sub>3</sub> (**325.08**): C, 66.36 (66.64); H, 4.02 (4.31); N, 12.90 (12.63).

*5.1.1.6. 2-Amino-4-(2,6-difluorophenyl)-5,6,7,8-tetrahydronaphthalene-1,3-dicarbonitrile (4d)*

Yield 80%, m.p. 215-217 °C. <sup>1</sup>H NMR (700 MHz, CDCl<sub>3</sub>):  $\delta$  1.61-1.63 (m, 2H, CH<sub>2</sub>), 1.72-1.74 (m, 2H, CH<sub>2</sub>), 2.15-2.17 (m, 2H, CH<sub>2</sub>), 2.87-2.89 (m, 2H, CH<sub>2</sub>), 6.64 (s, 2H, NH<sub>2</sub>, D<sub>2</sub>O-exchang.), 7.32-7.34 (m, 2H, Ar-H), 7.62-7.65 (m, 1H, Ar-H). <sup>13</sup>C NMR:  $\delta$  21.8, 22.1, 26.4, 29.4, 96.2, 97.9, 112.1-112.3 (dd,  $J = 6.3, 6.4$  Hz), 113.8 (t,  $J = 29.0$  Hz), 115.3 (d,  $J = 8.4$  Hz), 125.6, 131.7 (t,  $J = 14.0$  Hz), 137.9, 148.3, 151.2, 158.5 (d,  $J = 9.2$  Hz), 160.5 (d,  $J = 9.2$  Hz). ESI-MS,  $m/z$ : **310.2** [M+H]<sup>+</sup>. Anal. Calcd. (Found) for C<sub>18</sub>H<sub>13</sub>F<sub>2</sub>N<sub>3</sub> (**309.11**): C, 69.89 (70.11); H, 4.24 (4.57); N, 13.58 (13.23).

*5.1.1.7. 2-Amino-4-((1,1'-biphenyl)-4-yl)-5,6,7,8-tetrahydronaphthalene-1,3-dicarbonitrile (4e)*

Yield 90%, m.p. 251-253 °C. IR: 3416, 3307 (NH<sub>2</sub>); 2210 (2C≡N). <sup>1</sup>H NMR (400 MHz, DMSO-*d*<sub>6</sub>):  $\delta$  1.59-1.61 (m, 2H, CH<sub>2</sub>), 1.73-1.76 (m, 2H, CH<sub>2</sub>), 2.27 (t,  $J = 6.0$  Hz, 2H, CH<sub>2</sub>), 2.72 (t,  $J = 6.4$  Hz, 2H, CH<sub>2</sub>), 6.62 (s, 2H, NH<sub>2</sub>, D<sub>2</sub>O-exchang.), 7.36-7.43 (m, 3H, Ar-H), 7.51 (t,  $J = 7.6$  Hz, 2H, Ar-H), 7.76 (d,  $J = 7.2$  Hz, 2H, Ar-H), 7.81 (d,  $J = 8.4$  Hz, 2H, Ar-H). <sup>13</sup>C NMR:  $\delta$  22.6, 22.9, 26.6, 33.4, 89.9, 92.1, 116.7, 120.9, 127.2, 127.3, 127.4, 127.6, 128.7, 128.8, 134.9, 140.3, 141.7, 154.2, 157.1, 161.5. ESI-MS,  $m/z$ : **348.2** [M-H]<sup>+</sup>. Anal. Calcd. (Found) for C<sub>24</sub>H<sub>19</sub>N<sub>3</sub> (**349.16**): C, 82.49 (82.13); H, 5.48 (5.76); N, 12.03 (12.35).

5.1.1.8. *2-Amino-4-([1,3]benzodioxol-4-yl)-5,6,7,8-tetrahydronaphthalene-1,3-dicarbonitrile (4f)*

Yield 79%, m.p. 255-257 °C. IR: 3430, 3301 (NH<sub>2</sub>); 2212 (2C≡N). <sup>1</sup>H NMR (400 MHz, DMSO-*d*<sub>6</sub>): δ 1.60-1.64 (m, 2H, CH<sub>2</sub>), 1.72-1.75 (m, 2H, CH<sub>2</sub>), 2.35-2.19 (m, 2H, CH<sub>2</sub>), 2.71 (t, *J* = 6.0 Hz, 2H, CH<sub>2</sub>), 6.02 (s, 1H, Dioxole-H), 6.06 (s, 1H, Dioxole-H), 6.63 (s, 2H, NH<sub>2</sub>, D<sub>2</sub>O-exchang.), 6.75-6.77 (dd, *J* = 1.2, 1.2 Hz, 1H, Ar-H), 6.96 (t, *J* = 8.0 Hz, 1H, Ar-H), 7.02-7.04 (dd, *J* = 1.2, 1.2 Hz, 1H, Ar-H). <sup>13</sup>C NMR: δ 22.6, 22.8, 25.6, 33.2, 88.5, 101.6, 109.5, 116.9, 117.9, 119.4, 122.3, 122.5, 127.2, 127.7, 144.5, 147.7, 148.7, 158.4, 161.7. ESI-MS, *m/z*: 318.1 [M+H]<sup>+</sup>, 316.2 [M-H]<sup>+</sup>. Anal. Calcd. (Found) for C<sub>19</sub>H<sub>15</sub>N<sub>3</sub>O<sub>2</sub> (317.12): C, 71.91 (71.56); H, 4.76 (4.52); N, 13.24 (13.55).

5.1.1.9. *2-Amino-4-(naphthalen-2-yl)-5,6,7,8-tetrahydronaphthalene-1,3-dicarbonitrile (4g)*

Yield 87%, m.p. 220-222 °C. IR: 3408, 3306 (NH<sub>2</sub>); 2210 (2C≡N). <sup>1</sup>H NMR (400 MHz, CDCl<sub>3</sub>): δ 1.67-1.69 (m, 2H, CH<sub>2</sub>), 1.84-1.90 (m, 2H, CH<sub>2</sub>), 2.38-2.39 (m, 2H, CH<sub>2</sub>), 2.88 (t, *J* = 6.4 Hz, 2H, CH<sub>2</sub>), 5.32 (s, 2H, NH<sub>2</sub>, D<sub>2</sub>O-exchang.), 7.36-7.38 (dd, *J* = 1.6, 1.6 Hz, 1H, Ar-H), 7.56-7.58 (m, 2H, Ar-H), 7.77 (s, 1H, Ar-H), 7.89-7.93 (m, 2H, Ar-H), 7.98 (d, *J* = 8.4 Hz, 1H, Ar-H). <sup>13</sup>C NMR: δ 22.5, 22.8, 26.5, 33.3, 90.1, 90.2, 116.0, 120.7, 125.5, 126.6, 126.8, 127.6, 127.8, 128.2, 128.5, 133.5, 133.6, 154.4, 157.1, 161.5. ESI-MS, *m/z*: 324.1 [M+H]<sup>+</sup>. Anal. Calcd. (Found) for C<sub>22</sub>H<sub>17</sub>N<sub>3</sub> (323.14): C, 81.71 (81.43); H, 5.30 (5.67); N, 12.99 (12.67).

5.1.1.10. *2-Amino-4-(anthracen-9-yl)-5,6,7,8-tetrahydronaphthalene-1,3-dicarbonitrile (4h)*

Yield 85%, m.p. 296-299 °C. <sup>1</sup>H NMR (500 MHz, CDCl<sub>3</sub>): δ 1.49-1.57 (m, 2H, CH<sub>2</sub>), 1.82-1.86 (m, 2H, CH<sub>2</sub>), 1.95 (t, *J* = 6.5 Hz, 2H, CH<sub>2</sub>), 2.94 (t, *J* = 6.5 Hz, 2H, CH<sub>2</sub>), 5.19 (s, 2H, NH<sub>2</sub>, D<sub>2</sub>O-exchang.), 7.47-7.55 (m, 5H, Ar-H), 8.05-8.10 (m, 4H, Ar-H). <sup>13</sup>C NMR: δ 22.5, 25.3, 28.6, 33.4, 91.9, 106.7, 116.0, 121.1, 124.6, 125.4, 125.8, 125.9, 126.8, 127.4, 128.9, 131.2, 140.9, 152.3, 157.3, 157.4. ESI-MS, *m/z*: 374.2 [M+H]<sup>+</sup>. Anal. Calcd. (Found) for C<sub>26</sub>H<sub>19</sub>N<sub>3</sub> (373.16): C, 83.62 (83.93); H, 5.53 (5.37); N, 11.25 (11.58).

## 5.2. Biology

Detailed methods of biological assays are described in the [Supplementary file](#).

### 5.2.1. *In vitro* antitumor assay against cancer cells and cytotoxicity against normal cells

MTT assay was adopted for evaluation of antitumor activity against cancer cells and cytotoxicity against normal cells [42,43].

### 5.2.2. Mechanistic study

#### 5.2.2.1. Tubulin polymerization inhibition assay

Inhibition of tubulin polymerization was evaluated adopting the reported method [45,46].

#### 5.2.2.2. Flow cytometry assay

Flow cytometry assay was employed for assessment of cell cycle arrest in HepG2, HCT-116 and MCF-7 cancer cells according to the reported procedure [48-52].

#### 5.2.2.3. Caspases 3/9 assay

Levels of caspases 3 and 9 were assessed following the reported procedure [63].

## 5.3. Computational aided studies

### 5.3.1. Docking studies

The molecular docking calculations were done utilizing “molecular operating environment (MOE) version 2019.01” Chemical Computing Group Inc. software [65]. The crystal structure of tubulin (PDB code: 4O2B) complex was attained from the RCSB Protein Data Bank [64]. Energy minimization of compound **4c** was executed utilizing MMFF94x force field until a root-mean-square (RMS) gradient of 0.01 kcal/mol was reached. Additionally, all hydrogens were initially added and the forcefield partial charges were computed.

### 5.3.2. Molinspiration calculations

Molinspiration software [66] was utilized for analysis of Lipinski's rule parameters [67], TPSA and Nrotb of the new compounds [68]. Results (Supplementary Table S1) are described in the Supplementary file.

### 5.3.3. Prediction of toxicity risks in human and carcinogenicity in mice and rats

The new derivatives were analyzed for the prediction of various toxicity risks in human (tumorigenicity, irritancy and reproductive effects) using Osiris software [69], as well as carcinogenicity in mice and rats using PreADMET software [70]. Results (Supplementary Table S2) are described in the Supplementary file.

## Acknowledgments

Gratitude to Holding Company for Biological Products and Vaccines (VACSERA), Egypt for carrying out the cytotoxicity, tubulin polymerization inhibition, cell cycle analysis and caspases 3/9 assays.

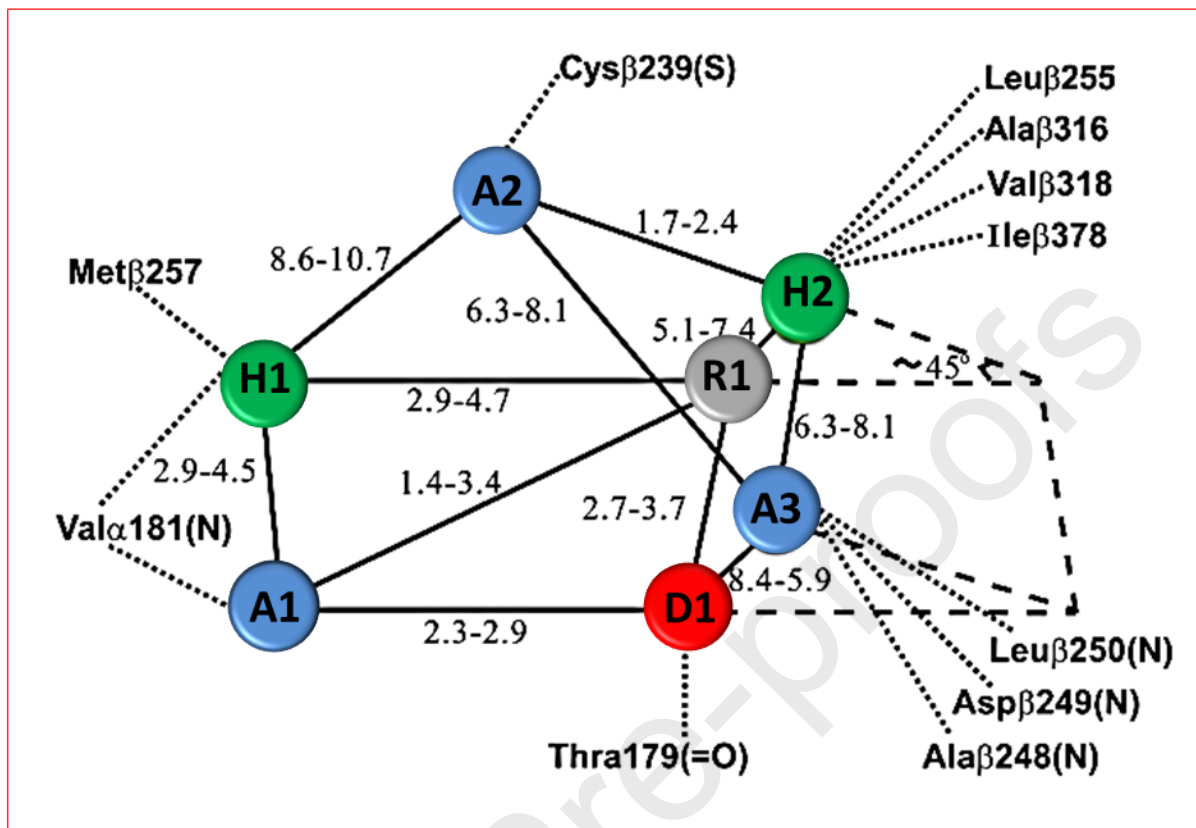


**Fig. 1.** Pharmacophoric features of CBSIs. The pharmacophoric points and distances between them are given in Å. Hydrogen bond acceptors (A1, A2, A3) are colored blue, Hydrogen bond donor (D1) is colored red, Hydrophobic centers (H1, H2) are colored green, and Planar moiety (R1) is colored grey.

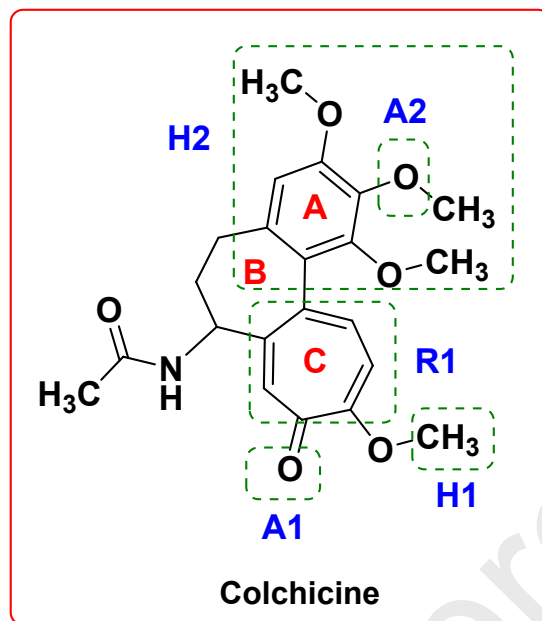


Fig. 2. The pharmacophoric features of colchicine.

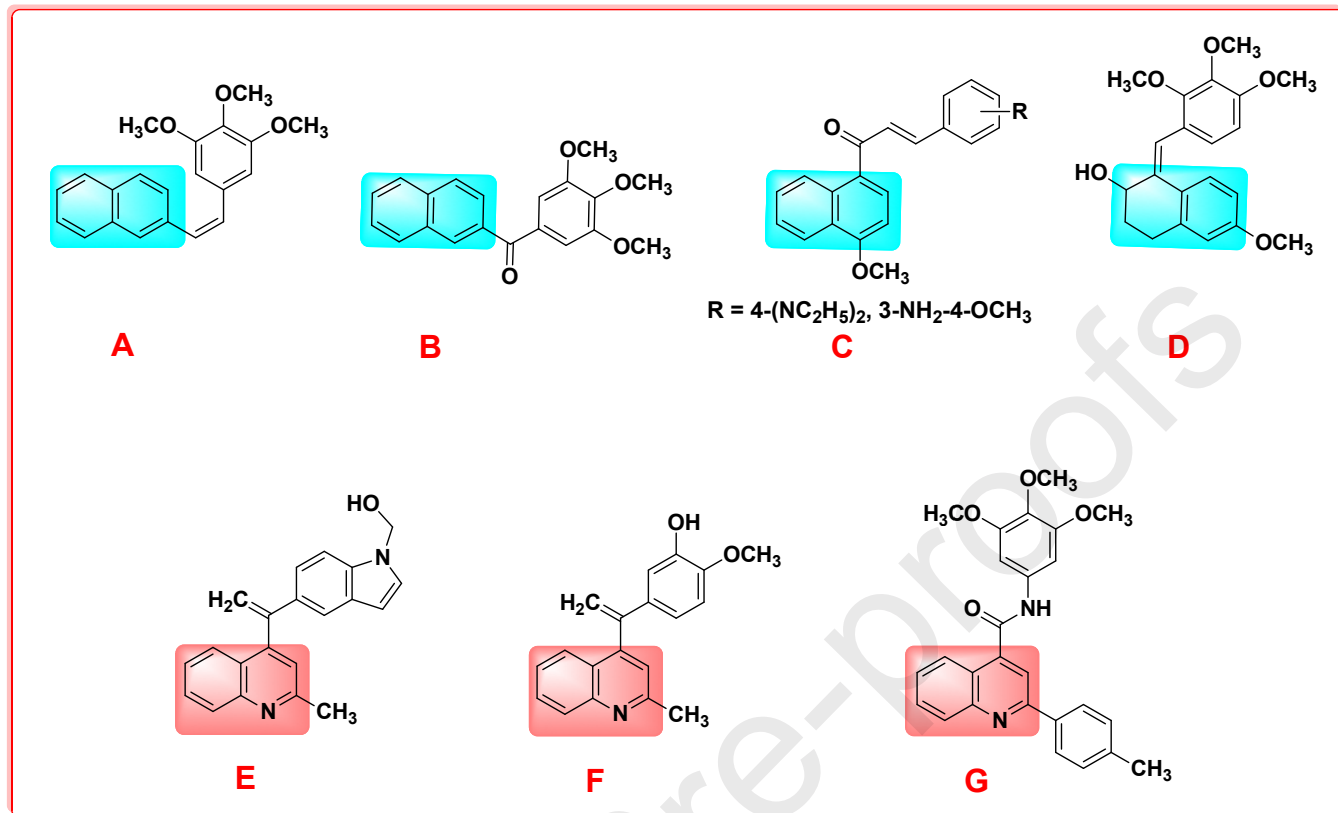
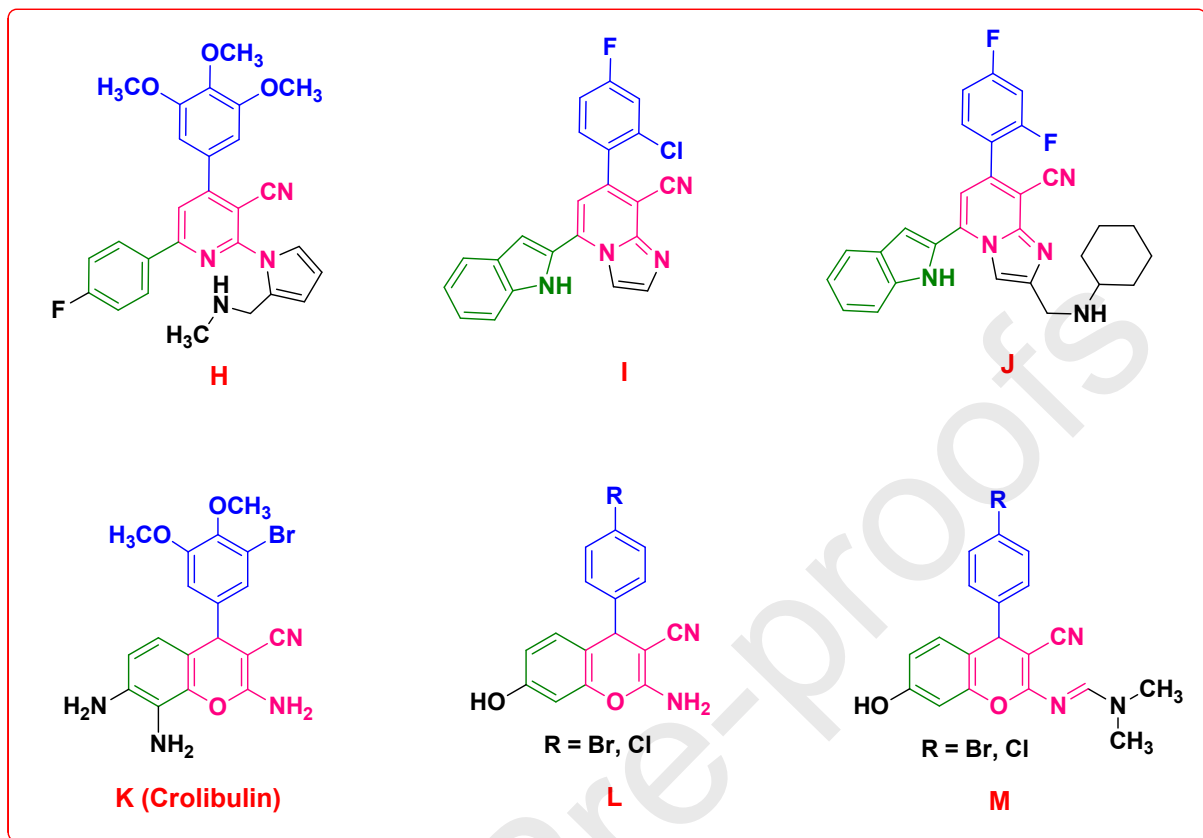
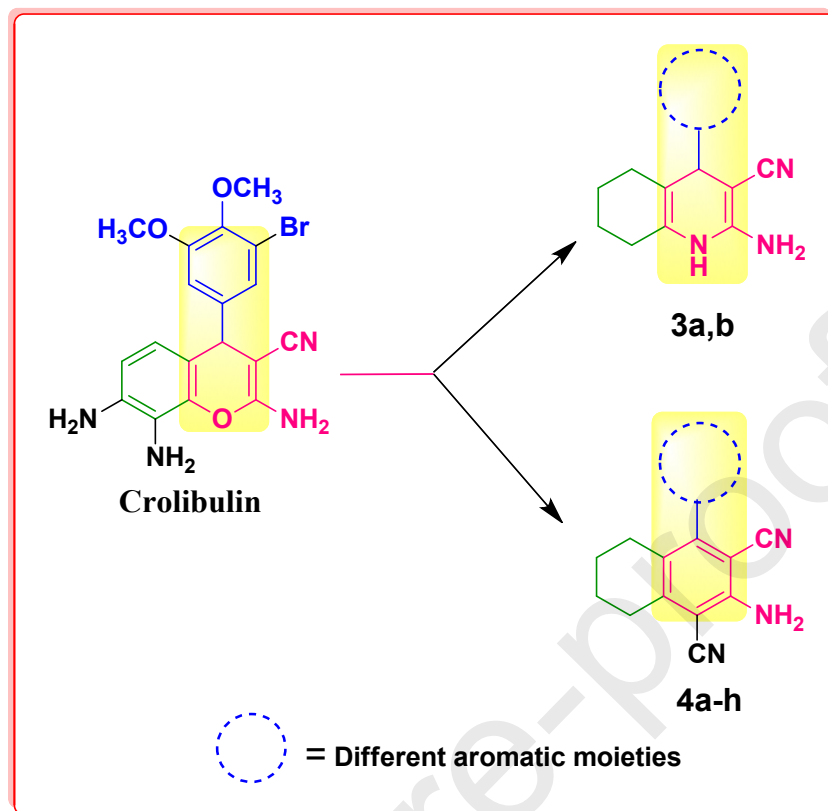


Fig. 3. Naphthalenes A-D and quinolines E-G with reported antitumor and tubulin polymerization inhibitory activities.



**Fig. 4.** 4,6-Diarylpyridine-3-carbonitrile **H**, 7-aryl-5-indolylimidazo[1,2-*a*]pyridine-8-carbonitriles **I**, **J** and 4-aryl-4*H*-chromenes **K-M** with reported antitumor and tubulin polymerization inhibitory activities.



**Fig. 5.** The designed new analogs **3a,b** and **4a-h** as potential antitumor agents and tubulin polymerization inhibitors.

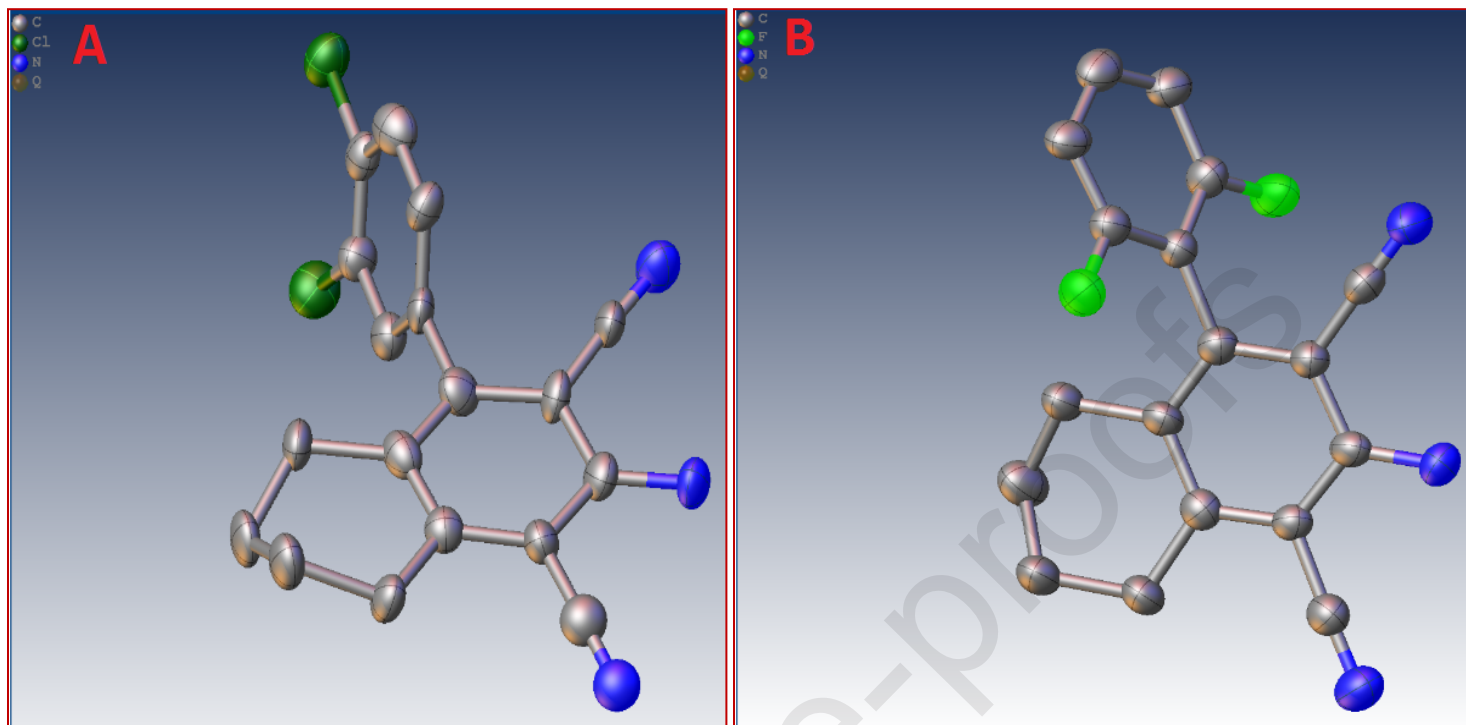


Fig. 6. The ORTEP plots of compounds **4b** (A) and **4d** (B).

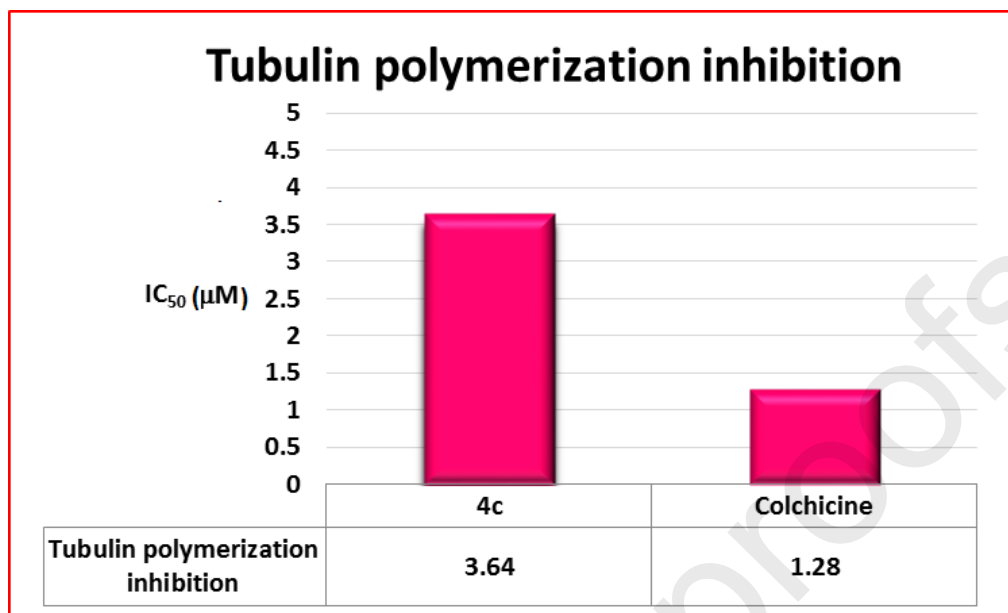
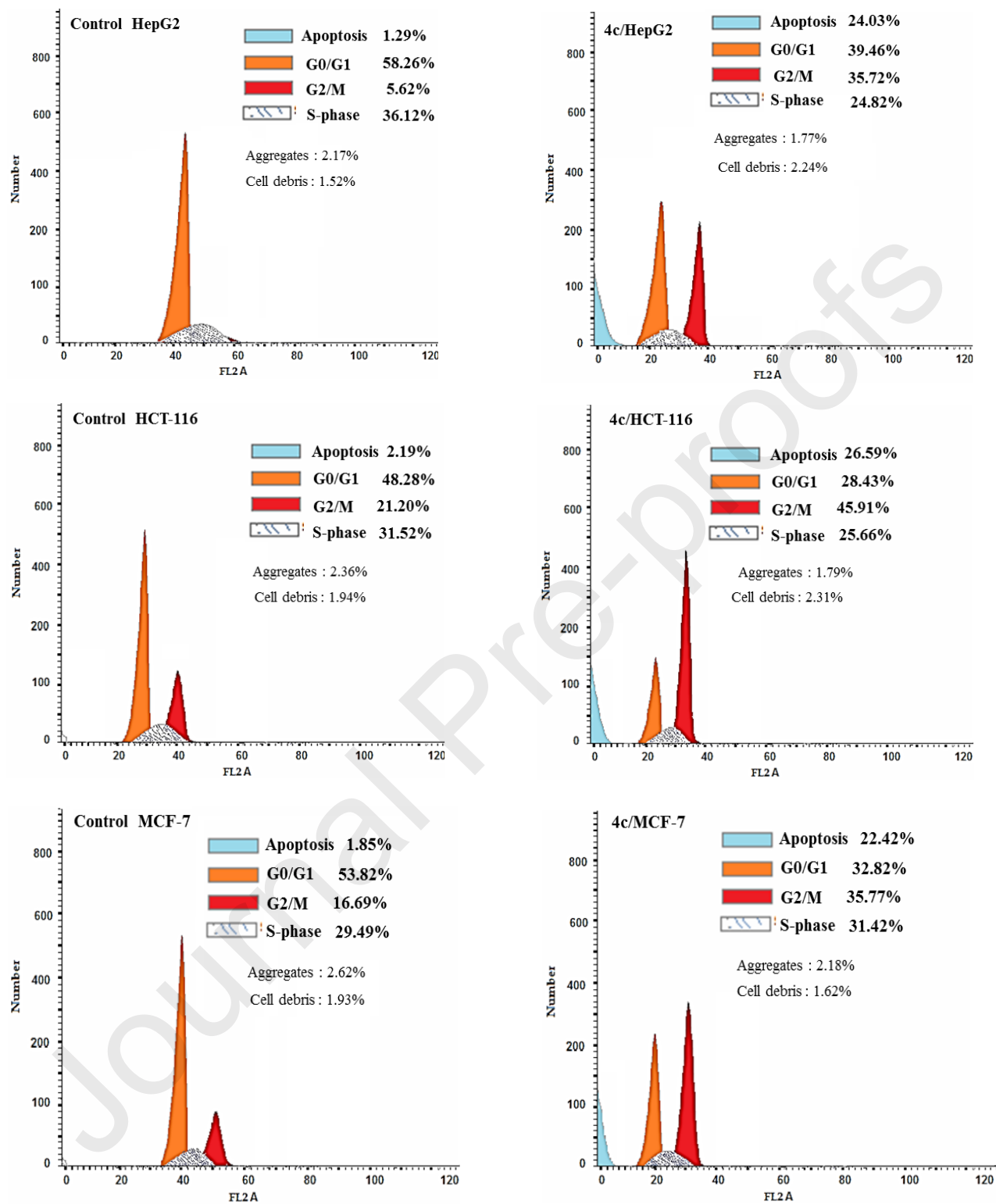
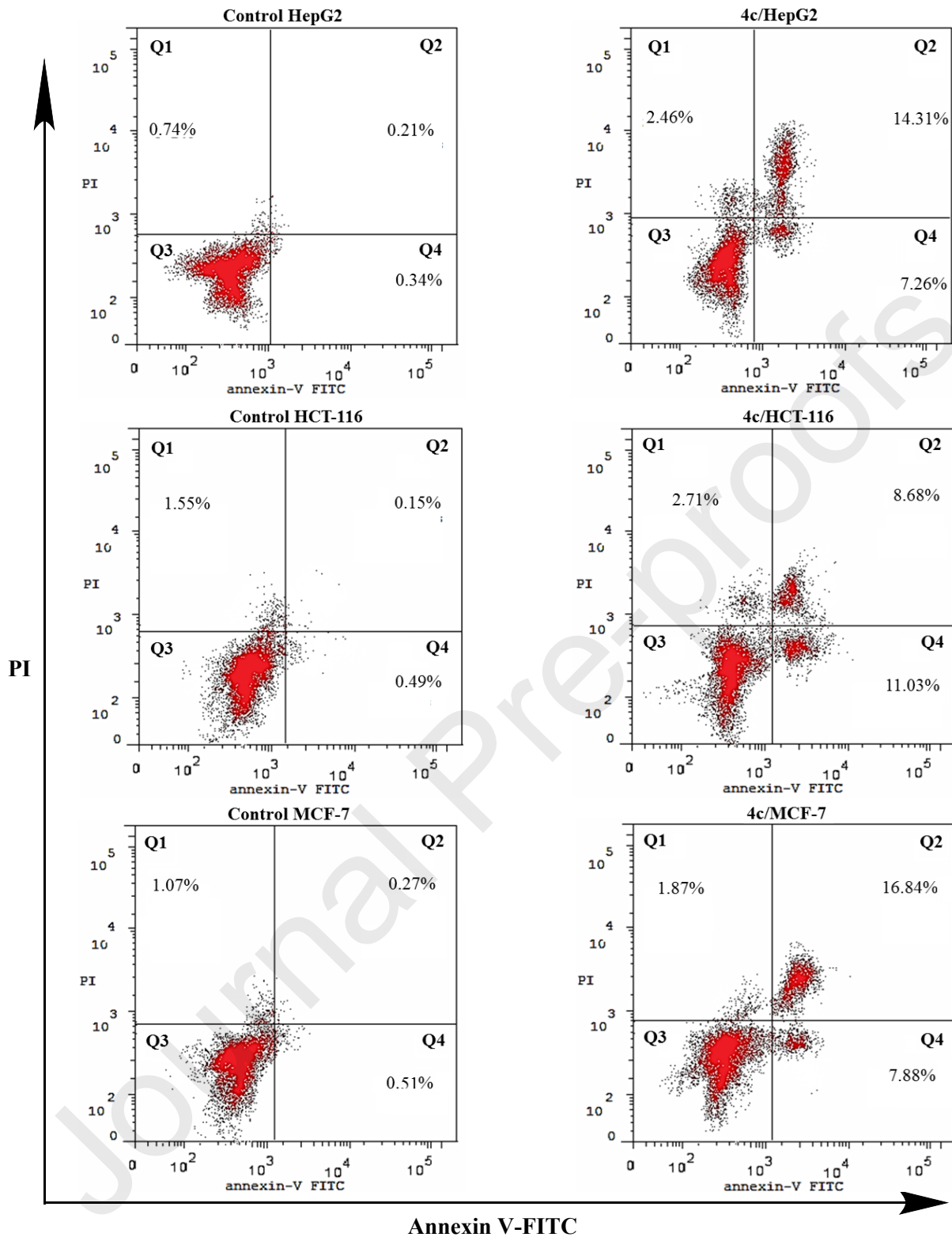


Fig. 7. Tubulin polymerization inhibition of 4c.



**Fig. 8.** Flow cytometric analysis of cell cycle phase distribution in HepG2, HCT-116 and MCF-7 cells after treatment with **4c** (at  $IC_{50}$  of the corresponding cell line) for 24 h.



**Fig. 9.** Annexin V-FITC/PI double staining for analysis of apoptosis in HepG2, HCT-116 and MCF-7 cells after treatment with 4c (at IC<sub>50</sub> of the corresponding cell line) for 24 h. Q1 quadrant points to dead (necrotic) cells; Q2 quadrant points to late apoptosis; Q3 quadrant points to live cells; Q4 quadrant points to early apoptosis. Total apoptosis is the summation of both early and late apoptosis.

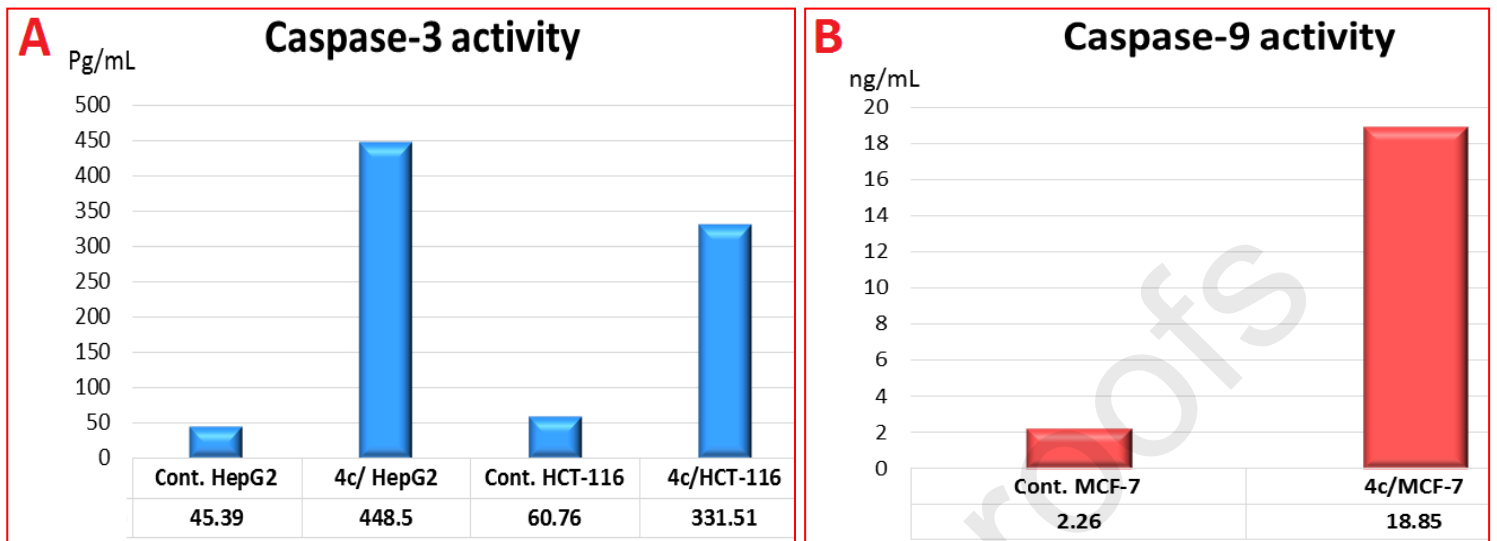


**Fig. 10.** (A) Results of caspase-3 induction in HepG2 and HCT-116 cells. (B) Results of caspase-9 induction in MCF-7 cells.

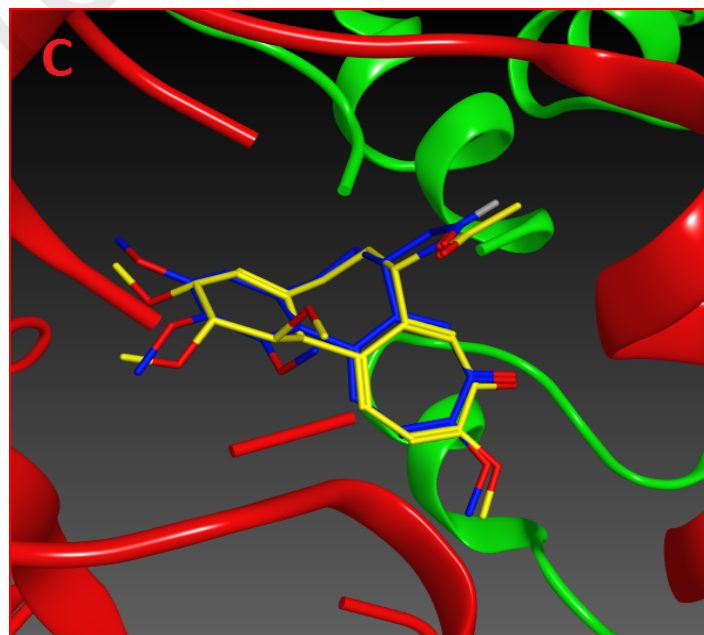
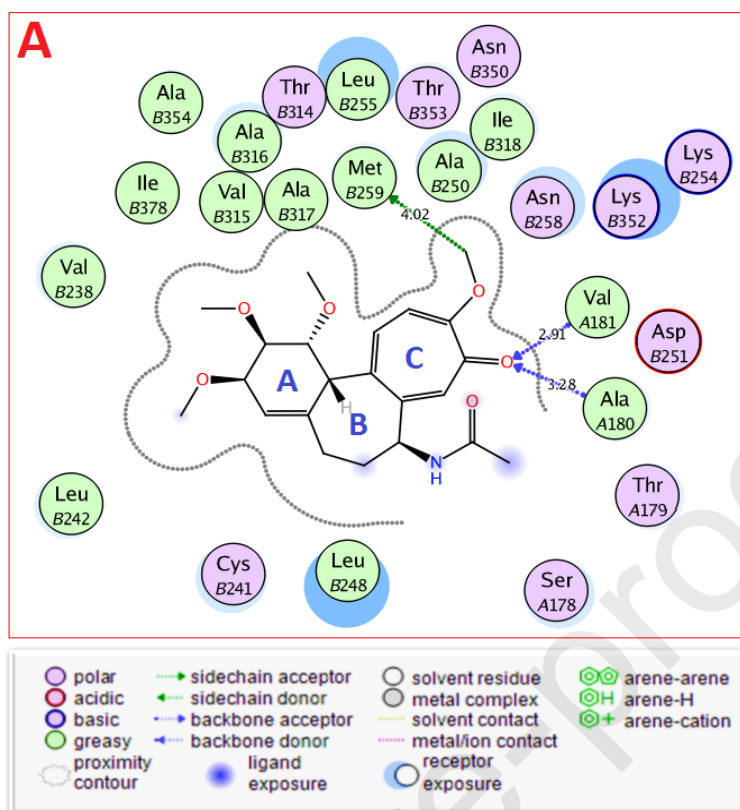


**Fig. 11.** (A) 2D Diagram of re-docked colchicine binding at the colchicine binding site of tubulin with bond distances (Å) shown. (B) 3D Diagram of the interaction between re-docked colchicine at the colchicine binding site. (C) Superimposition of the co-crystallized colchicine ligand (blue) and the docking pose of colchicine (yellow) at the colchicine binding site,  $\alpha$ -tubulin is colored green and  $\beta$ -tubulin is colored red. For clarity, some non-interacting residues are deleted. (PDB code: 4O2B).

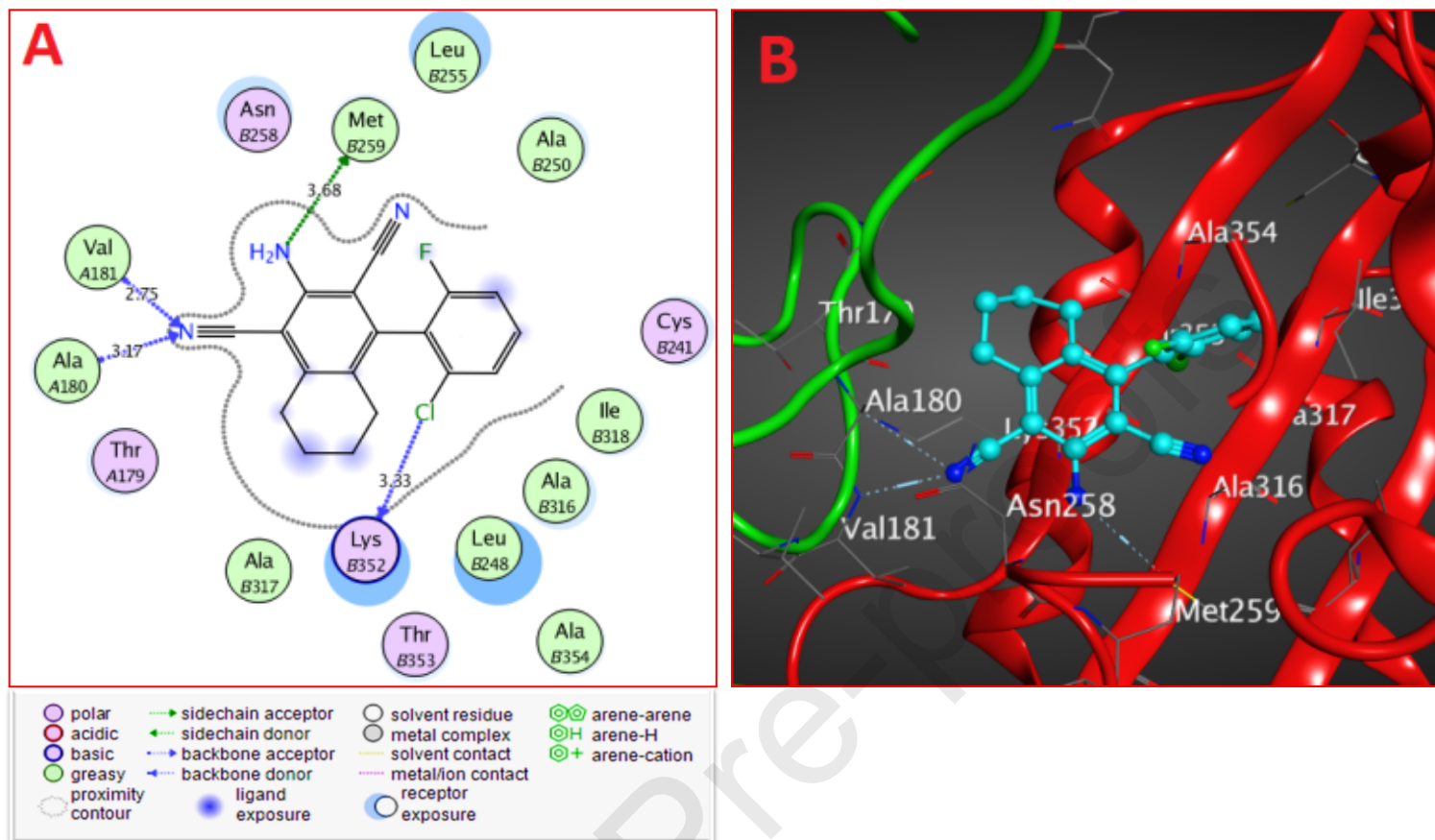


**Fig. 12.** (A) 2D Diagram of the interaction between **4c** and the colchicine binding site with bond distances (Å) shown. (B) 3D Diagram of the interaction between **4c** and the colchicine binding site. Compound **4c** is colored cyan,  $\alpha$ -tubulin is colored green and  $\beta$ -tubulin is colored red. For clarity, some non-interacting residues are deleted. (PDB code: 4O2B).

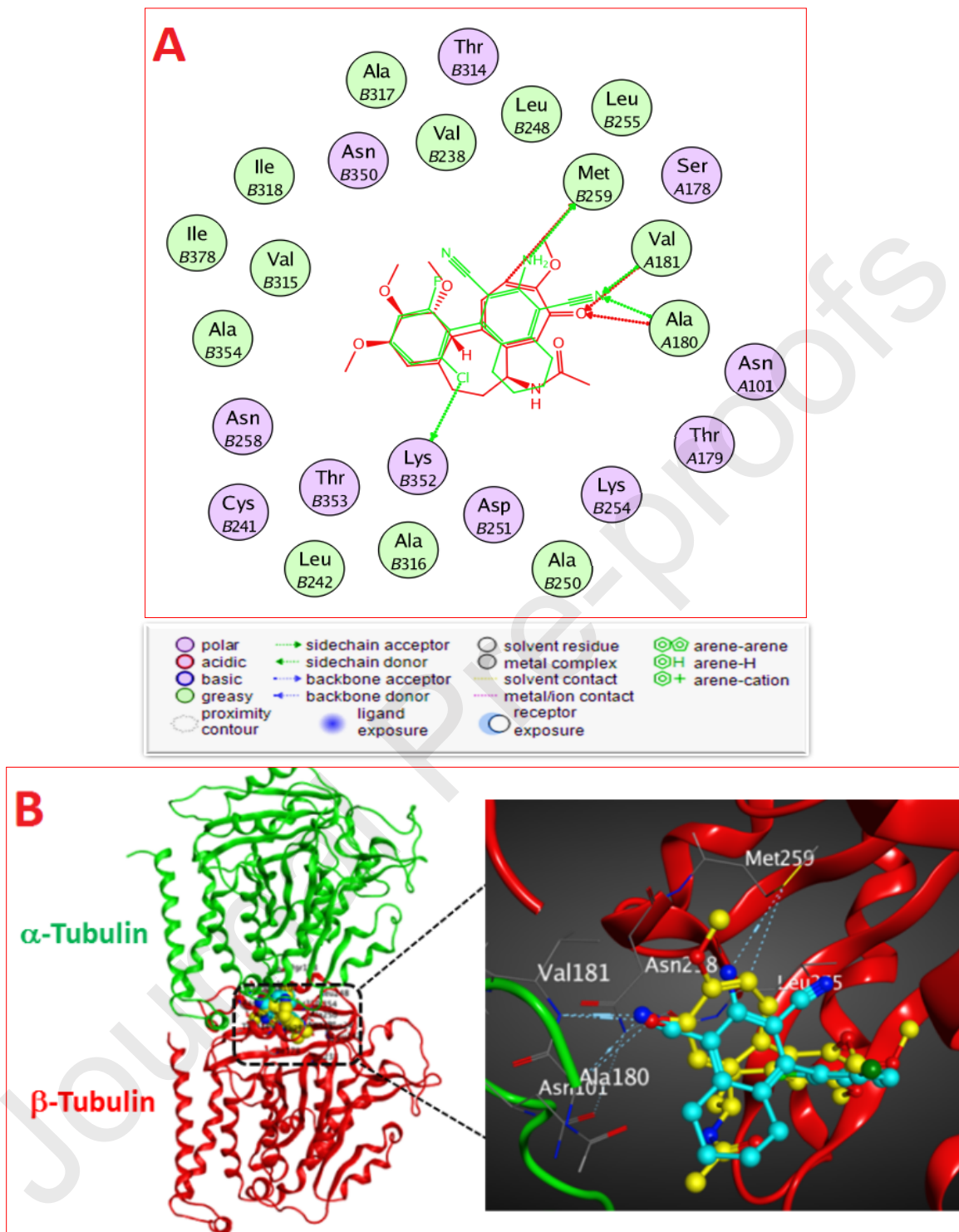


**Fig. 13.** (A) 2D Diagram of tubulin-4c binding mode superposed on tubulin-colchicine complex. Colchicine is colored red and 4c is colored green. (B) 3D Diagram of tubulin-4c binding mode superposed on tubulin-colchicine complex. Colchicine is colored yellow, 4c is colored cyan,  $\alpha$ -tubulin is colored green and  $\beta$ -tubulin is colored red. For clarity, some non-interacting residues are deleted. (PDB code: 4O2B).

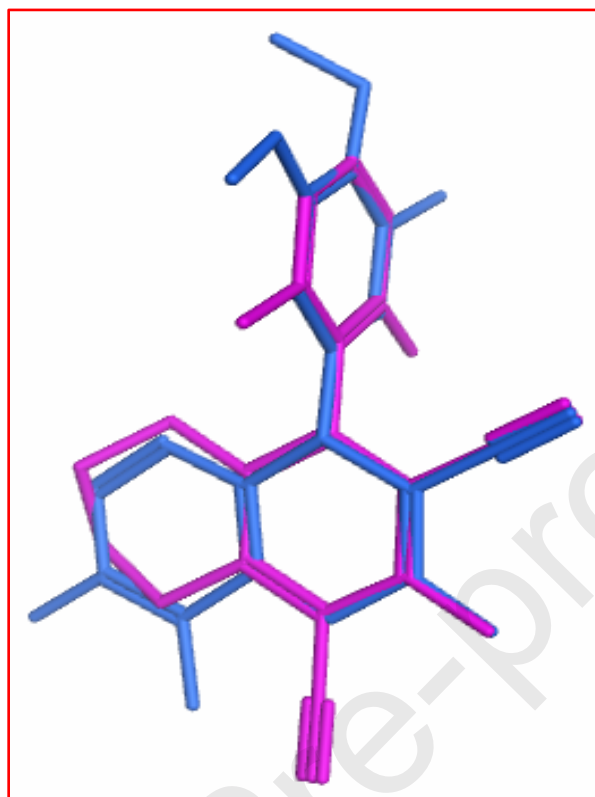


**Fig. 14.** Flexible alignment of **4c** (pink) and crolibulin (blue).

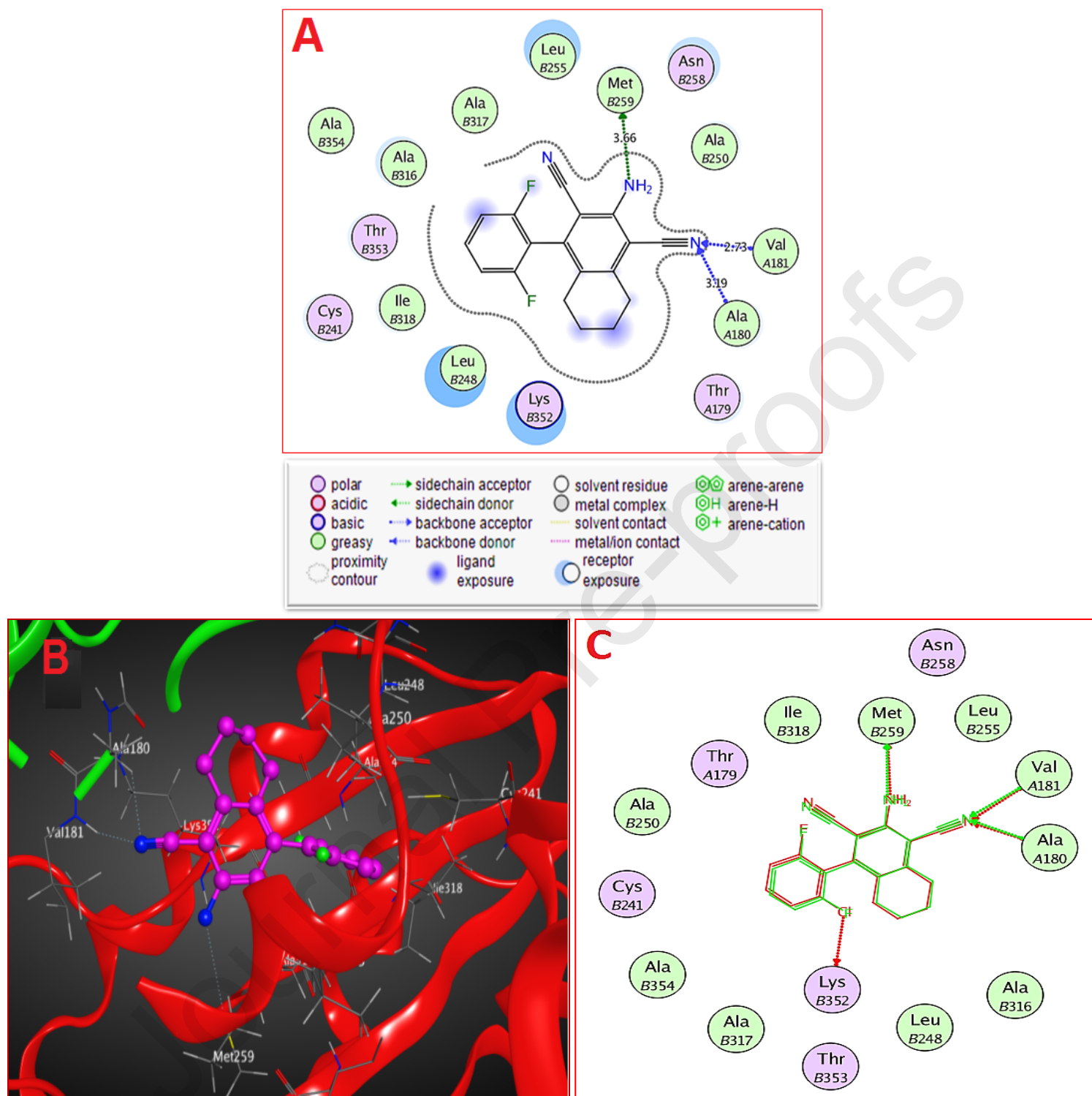


**Fig. 15.** (A) 2D Diagram of the interaction between **4d** and the colchicine binding site with bond distances ( $\text{\AA}$ ) shown. (B) 3D Diagram of the interaction between **4d** and the colchicine binding site. Compound **4d** is colored violet,  $\alpha$ -tubulin is colored green and  $\beta$ -tubulin is colored red. For clarity, some non-interacting residues are deleted. (C) 2D Diagram of **4c** and **4d** binding modes superposed on each other. Compound **4c** is colored red and **4d** is colored green (PDB code: 4O2B).

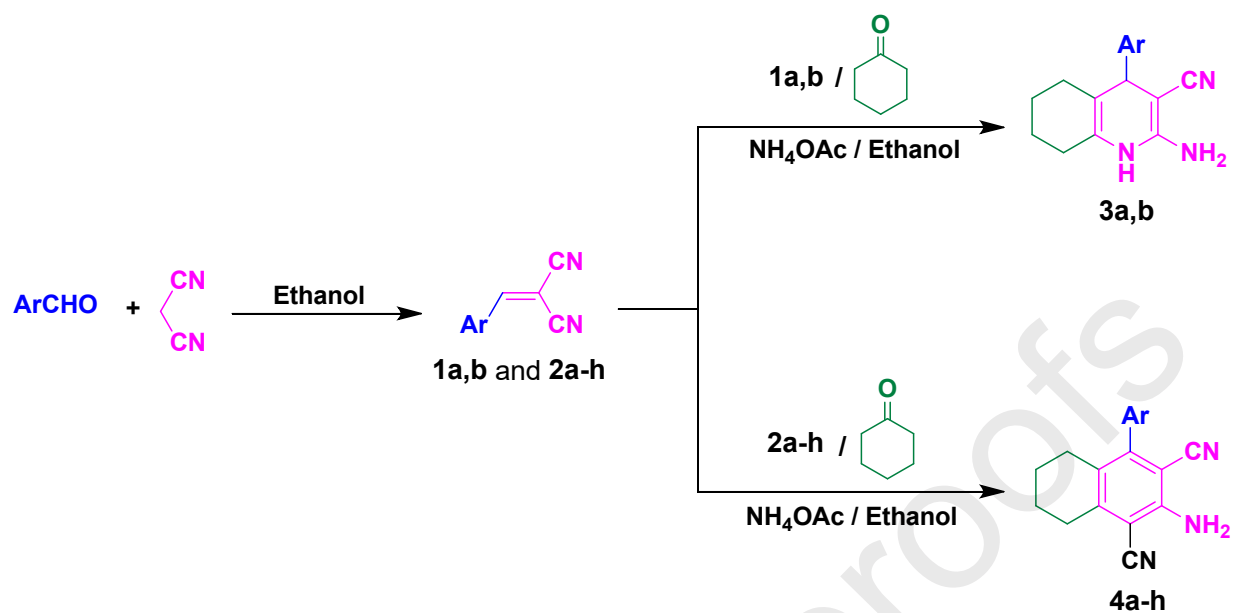
**Table 1.** *In vitro* antitumor assay results.

Comp. No.	IC <sub>50</sub> (μM) <sup>a,b</sup>		
	HepG2	HCT-116	MCF-7
<b>3a</b>	67.22±3.6	65.65±3.5	71.42±3.9
<b>3b</b>	39.02±2.4	36.56±2.4	58.98±3.4
<b>4a</b>	11.39±1.4	22.33±1.7	30.93±2.2
<b>4b</b>	26.80±2.1	12.40±1.1	<b>10.15±1.0</b>
<b>4c</b>	<b>6.02±0.5</b>	<b>8.45±1.0</b>	<b>6.28±0.6</b>
<b>4d</b>	82.29±4.8	90.78±4.9	>100.00
<b>4e</b>	82.65±5.1	85.33±4.6	90.67±4.9
<b>4f</b>	51.00±3.2	>100.00	>100.00
<b>4g</b>	19.92±1.7	17.33±1.5	17.36±1.9
<b>4h</b>	32.59±2.3	37.63±2.5	45.98±2.9
<b>Doxorubicin</b>	4.50±0.2	5.23±0.3	4.17±0.2
<b>Colchicine</b>	7.44±0.2	9.30±0.2	10.45±0.3

<sup>a</sup>IC<sub>50</sub> values = mean ± SD of three readings.

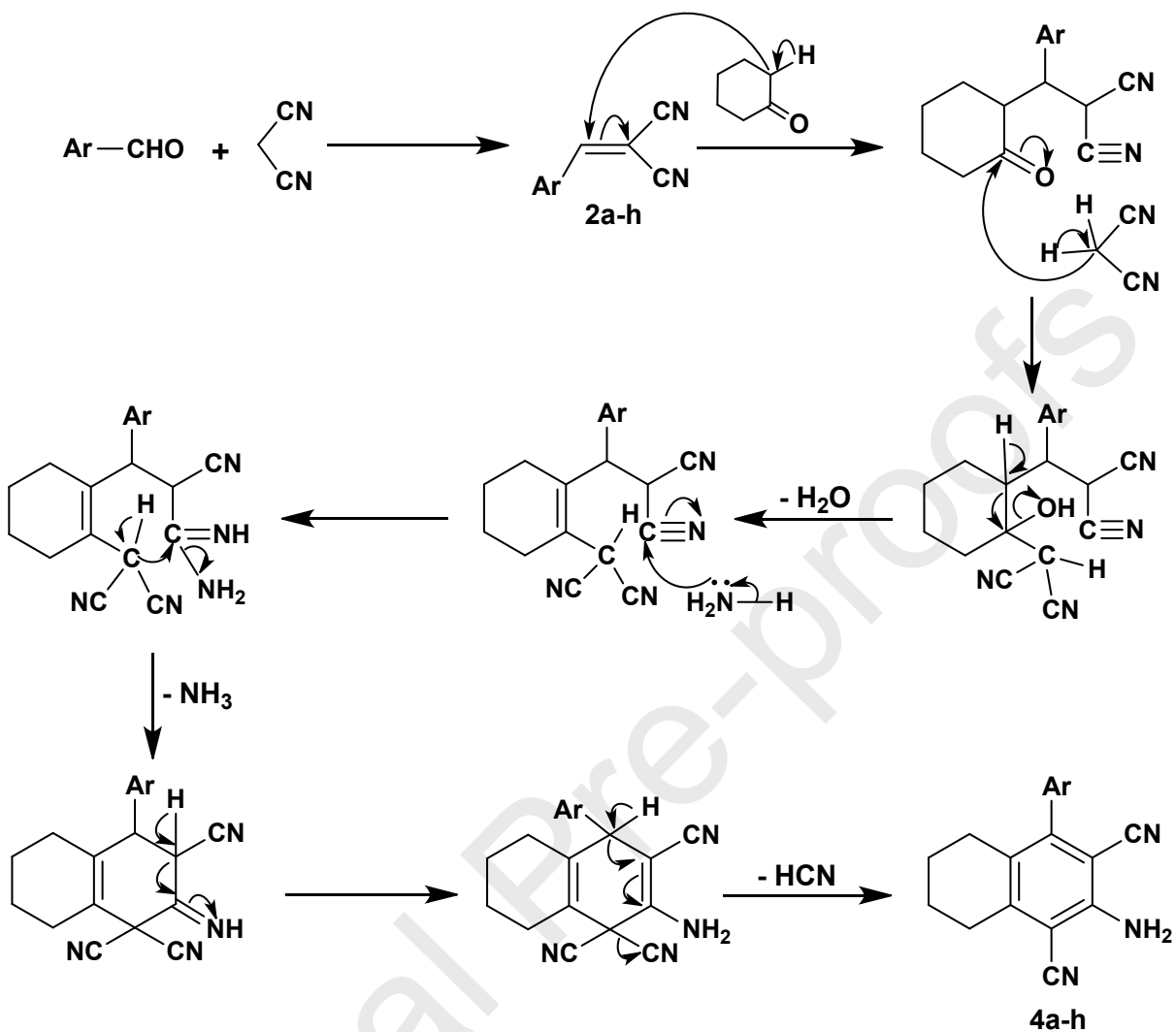
<sup>b</sup>IC<sub>50</sub> (μM): strong (1-10), moderate (11-50); weak (51-100); no activity (> 100).

Bold values refer to the good results.



Comp. No.	3a	3b	4a	4b	4c
Ar =					
Comp. No.	4d	4e	4f	4g	4h
Ar =					

Scheme 1. Synthesis of compounds 3a,b and 4a-h.



**Scheme 2.** The possible mechanism of the formation of 5,6,7,8-tetrahydronaphthalene-1,3-dicarbonitriles **4a-h**.

## References

- [1] J. Ferlay, M. Colombet, I. Soerjomataram, C. Mathers, D.M. Parkin, M. Piñeros, A. Znaor, F. Bray, Estimating the global cancer incidence and mortality in 2018: GLOBOCAN sources and methods, *Int. J. Cancer* 144 (2019) 1941–1953.
- [2] K. Westberg, G. Palmer, F. Hjern, T. Holm, A. Martling, Population-based study of surgical treatment with and without tumour resection in patients with locally recurrent rectal cancer, *Br. J. Surg.* 106 (2019) 790–798.
- [3] Y. Zhao, J. Cao, A. Melamed, M. Worley, A. Gockley, D. Jones, H.T. Nia, Y. Zhang, T. Stylianopoulos, A.S. Kumar, F. Mpekris, M. Datta, Y. Sun, L. Wu, X. Gao, O. Yeku, M. G.D. Carmen, D.R. Spriggs, R.K. Jain, L. Xu, Losartan treatment enhances chemotherapy efficacy and reduces ascites in ovarian cancer models by normalizing the tumor stroma, *Proc. Natl. Acad. Sci.* 116 (2019) 2210–2219.
- [4] M. Wells, E. King, K. Toft, F. MacAulay, J. Patterson, N. Dougall, N. Hulbert-Williams, S. Boa, E. Slaven, J. Cowie, J. McGarva, P.G. Niblock, J. Philp, J. Roe, Development and feasibility of a swallowing intervention package (SiP) for patients receiving radiotherapy treatment for head and neck cancer-the SiP study protocol, *Pilot Feasibility Stud.* 2 (2016) Article ID 40: 1-13.
- [5] J.C. Zabala, N.J. Cowan, Tubulin dimer formation *via* the release of  $\alpha$ - and  $\beta$ -tubulin monomers from multimolecular complexes, *Cell Motil.* 23 (1992) 222–230.
- [6] K.H. Downing, E. Nogales, Tubulin structure: Insights into microtubule properties and functions, *Curr. Opin. Struct. Biol.* 8 (1998) 785–791.
- [7] D. Fanale, G. Bronte, F. Passiglia, V. Calò, M. Castiglia, F. Di Piazza, N. Barraco, A. Cangemi, M.T. Catarella, L. Insalaco, A. Listi, R. Maragliano, D. Massihnia, A. Perez, F. Toia, G. Cicero, V. Bazan, Stabilizing versus destabilizing the microtubules: A double-edge sword for an effective cancer treatment option?, *Anal. Cell. Pathol.* 2015 (2015) Article ID 690916: 1-19.
- [8] T.L. Nguyen, C. McGrath, A.R. Hermone, J.C. Burnett, D.W. Zaharevitz, B.W. Day, P. Wipf, E. Hamel, R. Gussio, A common pharmacophore for a diverse set of colchicine site inhibitors using a structure-based approach, *J. Med. Chem.* 2005 (48) 6107–6116.
- [9] Y. Yin, B.-P. Lian, Y.-Z. Xia, Y.-Y. Shao, L.-Y. Kong, Design, synthesis and biological

- evaluation of resveratrol-cinnamoyl derivatives as tubulin polymerization inhibitors targeting the colchicine binding site, *Bioorg. Chem.* 93 (2019) Article ID 103319: 1-21.
- [10] R. Romagnoli, P. Oliva, M.K. Salvador, M.E. Camacho, C. Padroni, A. Brancale, S. Ferla, E. Hamel, R. Ronca, E. Grillo, R. Bortolozzi, F. Rruqa, E. Mariotto, G. Viola, Design, synthesis and biological evaluation of novel vicinal diaryl-substituted 1*H*-pyrazole analogues of combretastatin A-4 as highly potent tubulin polymerization inhibitors, *Eur. J. Med. Chem.* 181 (2019) Article ID 111577: 1-21.
- [11] M. Mustafa, S. Anwar, F. Elgamel, E.R. Ahmed, O.M. Aly, Potent combretastatin A-4 analogs containing 1,2,4-triazole: Synthesis, antiproliferative, anti-tubulin activity, and docking study, *Eur. J. Med. Chem.* 183 (2019) Article ID 111697: 1-12.
- [12] G. Wang, Z. Peng, Y. Li, Synthesis, anticancer activity and molecular modeling studies of novel chalcone derivatives containing indole and naphthalene moieties as tubulin polymerization inhibitors, *Chem. Pharm. Bull.* 67 (2019) 725-728.
- [13] G. Wang, Z. Peng, J. Zhang, J. Qiu, Z. Xie, Z. Gong, Synthesis, biological evaluation and molecular docking studies of aminochalcone derivatives as potential anticancer agents by targeting tubulin colchicine binding site, *Bioorg. Chem.* 78 (2018) 332–340.
- [14] G. Wang, J. Qiu, X. Xiao, A. Cao, F. Zhou, Synthesis, biological evaluation and molecular docking studies of a new series of chalcones containing naphthalene moiety as anticancer agents, *Bioorg. Chem.* 76 (2018) 249–257.
- [15] J. Jiang, C. Zheng, K. Zhu, J. Liu, N. Sun, C. Wang, H. Jiang, J. Zhu, C. Luo, Y. Zhou, Quantum chemistry calculation-aided structural optimization of combretastatin A-4-like tubulin polymerization inhibitors: Improved stability and biological activity, *J. Med. Chem.* 58 (2015) 2538–2546.
- [16] C. Álvarez, R. Álvarez, P. Corchete, C. Pérez-Melero, R. Peláez, M. Medarde, Naphthylphenstatins as tubulin ligands: Synthesis and biological evaluation, *Bioorg. Med. Chem.* 16 (2008) 8999-9008.
- [17] A.B.S. Maya, C. Pérez-Melero, C. Mateo, D. Alonso, J. L. Fernández, C. Gajate, F. Mollinedo, R. Peláez, E. Caballero, M. Medarde, Further naphthylcombretastatins. An investigation on the role of the naphthalene moiety, *J. Med. Chem.* 48 (2005) 556–568.

- [18] W. Li, W. Shuai, H. Sun, F. Xu, Y. Bi, J. Xu, C. Ma, H. Yao, Z. Zhu, S. Xu, Design, synthesis and biological evaluation of quinoline-indole derivatives as anti-tubulin agents targeting the colchicine binding site, *Eur. J. Med. Chem.* 163 (2019) 428–442.
- [19] A. Defant, I. Mancini, Design, synthesis and cancer cell growth inhibition evaluation of new aminoquinone hybrid molecules, *Molecules* 24 (2019) Article ID 24122224: 1-11.
- [20] L. Zhu, K. Luo, K. Li, Y. Jin, J. Lin, Design, synthesis and biological evaluation of 2-phenylquinoline-4-carboxamide derivatives as a new class of tubulin polymerization inhibitors, *Bioorg. Med. Chem.* 25 (2017) 5939–5951.
- [21] I. Khelifi, T. Naret, D. Renko, A. Hamze, G. Bernadat, J. Bignon, C. Lenoir, J. Dubois, J.-D. Brion, O. Provot, M. Alami, Design, synthesis and anticancer properties of isocombretaquinolines as potent tubulin assembly inhibitors, *Eur. J. Med. Chem.* 127 (2017) 1025–1034.
- [22] P.R. Kamath, D. Sunil, A.A. Ajees, Synthesis of indole-quinoline-oxadiazoles: Their anticancer potential and computational tubulin binding studies, *Res. Chem. Intermed.* 42 (2016) 5899–5914.
- [23] X.-F. Wang, S.-B. Wang, E. Ohkoshi, L.-T. Wang, E. Hamel, K. Qian, S.L. Morris-Natschke, K.-H. Lee, L. Xie, *N*-Aryl-6-methoxy-1,2,3,4-tetrahydroquinolines: A novel class of antitumor agents targeting the colchicine site on tubulin, *Eur. J. Med. Chem.* 67 (2013) 196–207.
- [24] Y. Liu, D. Yang, Z. Hong, S. Guo, M. Liu, D. Zuo, D. Ge, M. Qin, D. Sun, Synthesis and biological evaluation of 4,6-diphenyl-2-(1*H*-pyrrol-1-yl)nicotinonitrile analogues of crolibulin and combretastatin A-4, *Eur. J. Med. Chem.* 146 (2018) 185–193.
- [25] X. Zhai, X. Wang, J. Wang, J. Liu, D. Zuo, N. Jiang, T. Zeng, X. Yang, T. Jing, P. Gong, Discovery and optimization of novel 5-indolyl-7-arylimidazo[1,2-*a*]pyridine-8-carbonitrile derivatives as potent antitubulin agents targeting colchicine binding site, *Sci. Rep.* 7 (2017) Article ID 43398: 1-11.
- [26] J. Liu, D. Zuo, T. Jing, M. Guo, L. Xing, W. Zhang, J. Zhao, J. Shen, P. Gong, D. Zhang, X. Zhai, Synthesis, biological evaluation and molecular modeling of imidazo[1,2-*a*]pyridine derivatives as potent antitubulin agents, *Bioorg. Med. Chem.* 25 (2017) 4088–4099.

- [27] Z. Zhang, C. Wang, L. Ma, X. Jiang, C. Wu, Y. Wang, Y. Jiang, W. Zheng, Y. Yang, Y. Ma, J. Yang, Molecular mechanism of colibubulin in complex with tubulin provides a rationale for drug design, *Biochem. Biophys. Res. Commun.* 511 (2019) 381–386.
- [28] A.H. Halawa, M.M. Elaasser, A.M. El Kerdawy, A.M.A.I. Abd El-Hady, H.A. Emam, A. M. El-Agrody, Anticancer activities, molecular docking and structure–activity relationship of novel synthesized 4*H*-chromene, and 5*H*-chromeno[2,3-*d*]pyrimidine candidates, *Med. Chem. Res.* 26 (2017) 2624–2638.
- [29] W. Kemnitzer, J. Drewe, S. Jiang, H. Zhang, J. Zhao, C. Crogan-Grundy, L. Xu, S. Lamothe, H. Gourdeau, R. Denis, B. Tseng, S. Kasibhatla, X.C. Sui, Discovery of 4-aryl-4*H*-chromenes as a new series of apoptosis inducers using a cell- and caspase-based high-throughput screening assay. 3. Structure-activity relationships of fused rings at the 7,8-positions, *J. Med. Chem.* 50 (2007) 2858–2864.
- [30] G.B. Kharas, S.M. Russell, R. Cisler, T.L. Capen, E.A. Chlupsa, L.A. Debellis, J.T.A. Duke, C.B. Frazier, A. Gora, E. Kamenetsky, A.S. Kurani, D.L. Kuta, A.L. Madison, P. Miramon, Novel copolymers of vinyl acetate and halogen ring-disubstituted 2-phenyl-1,1-dicyanoethylenes, *J. Macromol. Sci. A* 45 (2008) 261–264.
- [31] S. Atlas, M. Raihane, G.B. Kharas, P.G. Hendrickson, H. Kaddami, M. Arous, A. Kallel, Novel copolymers of difluoro ring-substituted 2-phenyl-1,1-dicyanoethylenes with 4-fluorostyrene: Synthesis, structure and dielectric study, *J. Macromol. Sci. A* 49 (2012) 997–1010.
- [32] W. Fan, Y. Wang, Q. Zhang, A. Kirchon, Z. Xiao, L. Zhang, F. Dai, R. Wang, D. Sun, An amino-functionalized metal-organic framework, based on a rare  $\text{Ba}_{12}(\text{COO})_{18}(\text{NO}_3)_2$  cluster, for efficient  $\text{C}_3/\text{C}_2/\text{C}_1$  separation and preferential catalytic performance, *Chem. A Eur. J.* 24 (2018) 2137–2143.
- [33] B. Şen, E.H. Akdere, A. Şavk, E. Gültekin, Ö. Paralı, H. Göksu, F. Şen, A novel thiocarbamide functionalized graphene oxide supported bimetallic monodisperse Rh-Pt nanoparticles (RhPt/TC-GO NPs) for Knoevenagel condensation of aryl aldehydes together with malononitrile, *Appl. Catal. B Environ.* 225 (2018) 148–153.
- [34] R. Malakooti, H. Mahmoudi, R. Hosseinabadi, S. Petrov, A. Migliori, Facile synthesis of pure non-monoclinic zirconia nanoparticles and their catalytic activity investigations for

- Knoevenagel condensation, RSC Adv. 3 (2013) 22353–22359.
- [35] K. Turpaev, M. Ermolenko, T. Cresteil, J.C. Drapier, Benzylidenemalononitrile compounds as activators of cell resistance to oxidative stress and modulators of multiple signaling pathways. A structure-activity relationship study, *Biochem. Pharmacol.* 82 (2011) 535–547.
- [36] X.S. Wang, Z. Sen Zeng, Y.L. Li, D.Q. Shi, S.J. Tu, X.Y. Wei, Z.M. Zong, Simple procedure for the synthesis of arylmethylenemalononitrile without catalyst, *Synth. Commun.* 35 (2005) 1915–1920.
- [37] M.B. El-Ashmawy, M.A. El-Sherbeny, N.S. El-Gohary, Synthesis and antitumor screening of new series of pyrimido-[4,5-*b*]quinolines and [1,2,4]triazolo[2',3':3,4]pyrimido[6,5-*b*]quinolones, *Med. Chem. Res.* 22 (2013) 2724–2736.
- [38] A.O. Al-Youbi, A.M. Asiri, H.M. Faidallah, S.W. Ng, E.R.T. Tiekink, 3-Amino-1-(thiophen-2-yl)-9,10-dihydrophenanthrene-2,4-dicarbonitrile, *Acta Cryst.* E68 (2012) 1027–1028.
- [39] A.M. Asiri, H.M. Faidallah, K.A. Alamry, S.W. Ng, E.R.T. Tiekink, A second monoclinic polymorph for 3-amino-1-(4-methoxyphenyl)-9,10-dihydrophenanthrene-2,4-dicarbonitrile, *Acta Cryst.* E68 (2012) 1157–1158.
- [40] A.M. Asiri, H.M. Faidallah, A.O. Al-Youbi, S.W. Ng, 3-Amino-1-(4-bromophenyl)-9,10-dihydrophenanthrene-2,4-dicarbonitrile, *Acta Cryst.* E67 (2011) 920–925.
- [41] H.M. Faidallah, K.M.A. Al-Shaikh, T.R. Sobahi, K.A. Khan, A.M. Asiri, An efficient approach to the synthesis of highly congested 9,10-dihydrophenanthrene-2,4-dicarbonitriles and their biological evaluation as antimicrobial agents, *Molecules* 18 (2013) 15704–15716.
- [42] F. Denizot, R. Lang, Rapid colorimetric assay for cell growth and survival. Modifications to the tetrazolium dye procedure giving improved sensitivity and reliability, *J. Immunol. Methods* 89 (1986) 271–277.
- [43] D. Gerlier, N. Thomasset, Use of MTT colorimetric assay to measure cell activation, *J. Immunol. Methods* 94 (1986) 57–63.
- [44] M.R. Scholfield, C.M. Zanden, M. Carter, P.S. Ho, Halogen bonding (X-bonding): A

- biological perspective, *Protein Sci.* 22 (2013) 139–152.
- [45] J.F. Díaz, J.M. Andreu, Assembly of purified GDP-tubulin into microtubules induced by taxol and taxotere: Reversibility, ligand stoichiometry, and competition, *Biochemistry* 32 (1993) 2747–2755.
- [46] R.I. Ahmed, E.E.A. Osman, F.M. Awadallah, S.M. El-Moghazy, Design, synthesis and molecular docking of novel diarylcyclohexenone and diarylindazole derivatives as tubulin polymerization inhibitors, *J. Enzyme Inhib. Med. Chem.* 32 (2017) 176–188.
- [47] Y.L. Zhang, B.Y. Li, R. Yang, L.Y. Xia, A.L. Fan, Y.C. Chu, L.J. Wang, Z.C. Wang, A.Q. Jiang, H.L. Zhu, A class of novel tubulin polymerization inhibitors exert effective anti-tumor activity *via* mitotic catastrophe, *Eur. J. Med. Chem.* 12 (2019) 896–910.
- [48] M. Xu, Y. Xu, Y. Shen, C. Lou, M. Zheng, J. Kang, Determining the affinity of anti-mitotic compounds binding to colchicine binding site of tubulin by affinity probe capillary electrophoresis, *J. Chromatogr. B.* 1121 (2019) 66–71.
- [49] E. Lee, Y.J. Surh, Induction of apoptosis in HL-60 cells by pungent vanilloids, [6]-gingerol and [6]-paradol, *Cancer Lett.* 134 (1998) 163–168.
- [50] Y.C. Li, Y.S. Tyan, H.M. Kuo, W.C. Chang, T.C. Hsia, J.G. Chung, Baicalein induced *in vitro* apoptosis undergo caspases activity in human promyelocytic leukemia HL-60 cells, *Food Chem. Toxicol.* 42 (2004) 37–43.
- [51] K.K.W. Lo, T.K.M. Lee, J.S.Y. Lau, W.L. Poon, S.H. Cheng, Luminescent biological probes derived from ruthenium(II) estradiol polypyridine complexes, *Inorg. Chem.* 47 (2008) 200–208.
- [52] C.S. Devi, D.A. Kumar, S.S. Singh, N. Gabra, N. Deepika, Y.P. Kumar, S. Satyanarayana, Synthesis, interaction with DNA, cytotoxicity, cell cycle arrest and apoptotic inducing properties of ruthenium(II) molecular “light switch” complexes, *Eur. J. Med. Chem.* 64 (2013) 410–421.
- [53] R.S.Y. Wong, Apoptosis in cancer: From pathogenesis to treatment, *J. Exp. Clin. Cancer Res.* 30 (2011) Article ID 87: 1-14.
- [54] K. Hara, E. Kasahara, N. Takahashi, M. Konishi, J. Inoue, M. Jikumaru, S. Kubo, H. Okamura, E. Sato, M. Inoue, Mitochondria determine the efficacy of anticancer agents

- that interact with DNA but not the cytoskeleton, *J. Pharmacol. Exp. Ther.* 337 (2011) 838-845.
- [55] K.S.-O.U. Fischer, R. Jänicke, Many cuts to ruin: A comprehensive update of caspase substrates, *Cell Death Differ.* 10 (2003) 76-100.
- [56] M. Olsson, B. Zhivotovsky, Caspase and cancer, *Cell Death Differ.* 18 (2011) 1441–1449.
- [57] C. Tang, Y.H. Lu, J.H. Xie, F. Wang, J.N. Zou, J.S. Yang, Y.Y. Xing, T. Xi, Downregulation of survivin and activation of caspase-3 through the PI3K/Akt pathway in ursolic acid-induced HepG2 cell apoptosis, *Anticancer Drugs* 20 (2009) 249–258.
- [58] M. Zhou, X. Liu, Z. Li, Q. Huang, F. Li, C.Y. Li, Caspase-3 regulates the migration, invasion and metastasis of colon cancer cells, *Int. J. Cancer* 143 (2018) 921–930.
- [59] R.U. Jänicke, MCF-7 breast carcinoma cells do not express caspase-3, *Breast Cancer Res. Treat.* 117 (2009) 219–221.
- [60] S. Kagawa, J. Gu, T. Honda, T.J. McDonnell, S.G. Swisher, J.A. Roth, B. Fang, Deficiency of caspase-3 in MCF7 cells blocks Bax-mediated nuclear fragmentation but not cell death 1, *Clin. Cancer Res.* 7 (2001) 1474–1480.
- [61] H. Thomadaki, M. Talieri, A. Scorilas, Treatment of MCF-7 cells with taxol and etoposide induces distinct alterations in the expression of apoptosis-related genes BCL2, BCL2L12, BAX, CASPASE-9 and FAS, *Biol. Chem.* 387 (2006) 1081–1086.
- [62] Q. Cui, J.H. Yu, J.N. Wu, S.I. Tashiro, S. Onodera, M. Minami, T. Ikejima, P53-mediated cell cycle arrest and apoptosis through a caspase-3- independent, but caspase-9-dependent pathway in oridonin-treated MCF-7 human breast cancer cells, *Acta Pharmacol. Sin.* 28 (2007) 1057–1066.
- [63] P.D. Mace, S.J. Riedl, G.S. Salvesen, Caspase enzymology and activation mechanisms. In "Methods in Enzymology", A. Ashkenazi, J. Yuan, J.A. Wells (eds.), 1<sup>st</sup> Ed., Elsevier Inc., (2014) Chapter 7, 162-178.
- [64] <https://www.rcsb.org/structure/4o2b>.
- [65] Molecular Operating Environment (MOE), 2019.01; Chemical Computing Group ULC, 1010 Sherbrooke St. West, Montreal, QC, Canada, H3A 2R7, 2019, <https://www.chemcomp.com/>.

- [66] <http://www.molinspiration.com/cgi-bin/properties>.
- [67] C.A. Lipinski, Lead- and drug-like compounds: The rule-of-five revolution, *Drug Discov. Today Technol.* 1 (2004) 337–341.
- [68] D.F. Veber, S.R. Johnson, H.Y. Cheng, B.R. Smith, K.W. Ward, K.D. Kopple, Molecular properties that influence the oral bioavailability of drug candidates, *J. Med. Chem.* 45 (2002) 2615–2623.
- [69] <https://www.organic-chemistry.org/prog/peo/>.
- [70] <https://preadmet.bmdrc.kr>.

### Captions of Figures, Tables and Schemes

**Fig. 1.** Pharmacophoric features of CBSIs. The pharmacophoric points and distances between them are given in Å. Hydrogen bond acceptors (A1, A2, A3) are colored blue, Hydrogen bond donor (D1) is colored red, Hydrophobic centers (H1, H2) are colored green, and Planar moiety (R1) is colored grey.

**Fig. 2.** The pharmacophoric features of colchicine.

**Fig. 3.** Naphthalenes **A-D** and quinolines **E-G** with reported antitumor and tubulin polymerization inhibitory activities.

**Fig. 4.** 4,6-Diarylpyridine-3-carbonitrile **H**, 7-aryl-5-indolyimidazo[1,2-*a*]pyridine-8-carbonitriles **I, J** and 4-aryl-4*H*-chromenes **K-M** with reported antitumor and tubulin polymerization inhibitory activities.

**Fig. 5.** The designed new analogs **3a,b** and **4a-h** as potential antitumor agents and tubulin polymerization inhibitors.

**Fig. 6.** The ORTEP plots of compounds **4b** (A) and **4d** (B).

**Fig. 7.** Tubulin polymerization inhibition of **4c**.

**Fig. 8.** Flow cytometric analysis of cell cycle phase distribution in HepG2, HCT-116 and MCF-7 cells after treatment with **4c** (at IC<sub>50</sub> of the corresponding cell line) for 24 h.

**Fig. 9.** Annexin V-FITC/PI double staining for analysis of apoptosis in HepG2, HCT-116 and MCF-7 cells after treatment with **4c** (at IC<sub>50</sub> of the corresponding cell line) for 24 h. Q1 quadrant points to dead (necrotic) cells; Q2 quadrant points to late apoptosis; Q3 quadrant points to live cells; Q4 quadrant points to early apoptosis. Total apoptosis is the summation of both early and late apoptosis.

**Fig. 10.** (A) Results of caspase-3 induction in HepG2 and HCT-116 cancer cells. (B) Results of caspase-9 induction in MCF-7 cancer cells.

**Fig. 11.** (A) 2D Diagram of re-docked colchicine binding at the colchicine binding site of tubulin with bond distances (Å) shown. (B) 3D Diagram of the interaction between re-docked colchicine

at the colchicine binding site. (C) Superimposition of the co-crystallized colchicine ligand (blue) and the docking pose of colchicine (yellow) at the colchicine binding site,  $\alpha$ -tubulin is colored green and  $\beta$ -tubulin is colored red. For clarity, some non-interacting residues are deleted. (PDB code: 4O2B).

**Fig. 12.** (A) 2D Diagram of the interaction between **4c** and the colchicine binding site with bond distances ( $\text{Å}$ ) shown. (B) 3D Diagram of the interaction between **4c** and the colchicine binding site. Compound **4c** is colored cyan,  $\alpha$ -tubulin is colored green and  $\beta$ -tubulin is colored red. For clarity, some non-interacting residues are deleted. (PDB code: 4O2B).

**Fig. 13.** (A) 2D Diagram of tubulin-**4c** binding mode superposed on tubulin-colchicine complex. Colchicine is colored red and **4c** is colored green. (B) 3D Diagram of tubulin-**4c** binding mode superposed on tubulin-colchicine complex. Colchicine is colored yellow, **4c** is colored cyan,  $\alpha$ -tubulin is colored green and  $\beta$ -tubulin is colored red. For clarity, some non-interacting residues are deleted. (PDB code: 4O2B)

**Fig. 14.** Flexible alignment of **4c** (pink) and colibulin (blue).

**Fig. 15.** (A) 2D Diagram of the interaction between **4d** and the colchicine binding site with bond distances ( $\text{Å}$ ) shown. (B) 3D Diagram of the interaction between **4d** and the colchicine binding site. Compound **4d** is colored violet,  $\alpha$ -tubulin is colored green and  $\beta$ -tubulin is colored red. For clarity, some non-interacting residues are deleted. (C) 2D Diagram of **4c** and **4d** binding modes superposed on each other. Compound **4c** is colored red and **4d** is colored green (PDB code: 4O2B).

**Supplementary Fig. S1.** The ORTEP plots of 2-(2,3-dichlorobenzylidene)malononitrile (**1a**) (A) and 2-([1,1'-biphenyl]-4-ylmethylene)malononitrile (**2e**) (B).

**Table 1.** *In vitro* antitumor testing results.

**Supplementary Table S1.** TPSA, Nrotb and calculated Lipinski's rule for compounds **3a,b** and **4a-h**.

**Supplementary Table S2.** *In silico* prediction of toxicity risks in human and carcinogenicity in animals.

**Scheme 1.** Synthesis of compounds **3a,b** and **4a-h**.

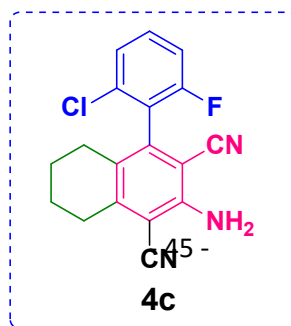
**Scheme 2.** The possible mechanism of the formation of 5,6,7,8-tetrahydronaphthalene-1,3-dicarbonitriles **4a-h**.

- New hexahydroquinolines and tetrahydronaphthalenes were prepared.
- The new analogs were screened for antitumor activity
- Analog **4c** showed the highest antitumor activity
- Analog **4c** showed good tubulin polymerization inhibitory activity
- Analog **4c** induced cell cycle arrest at G2/M and pre-G1 phases
- Analog **4c** induced cell death through apoptosis supported by increased levels of caspases 3/9

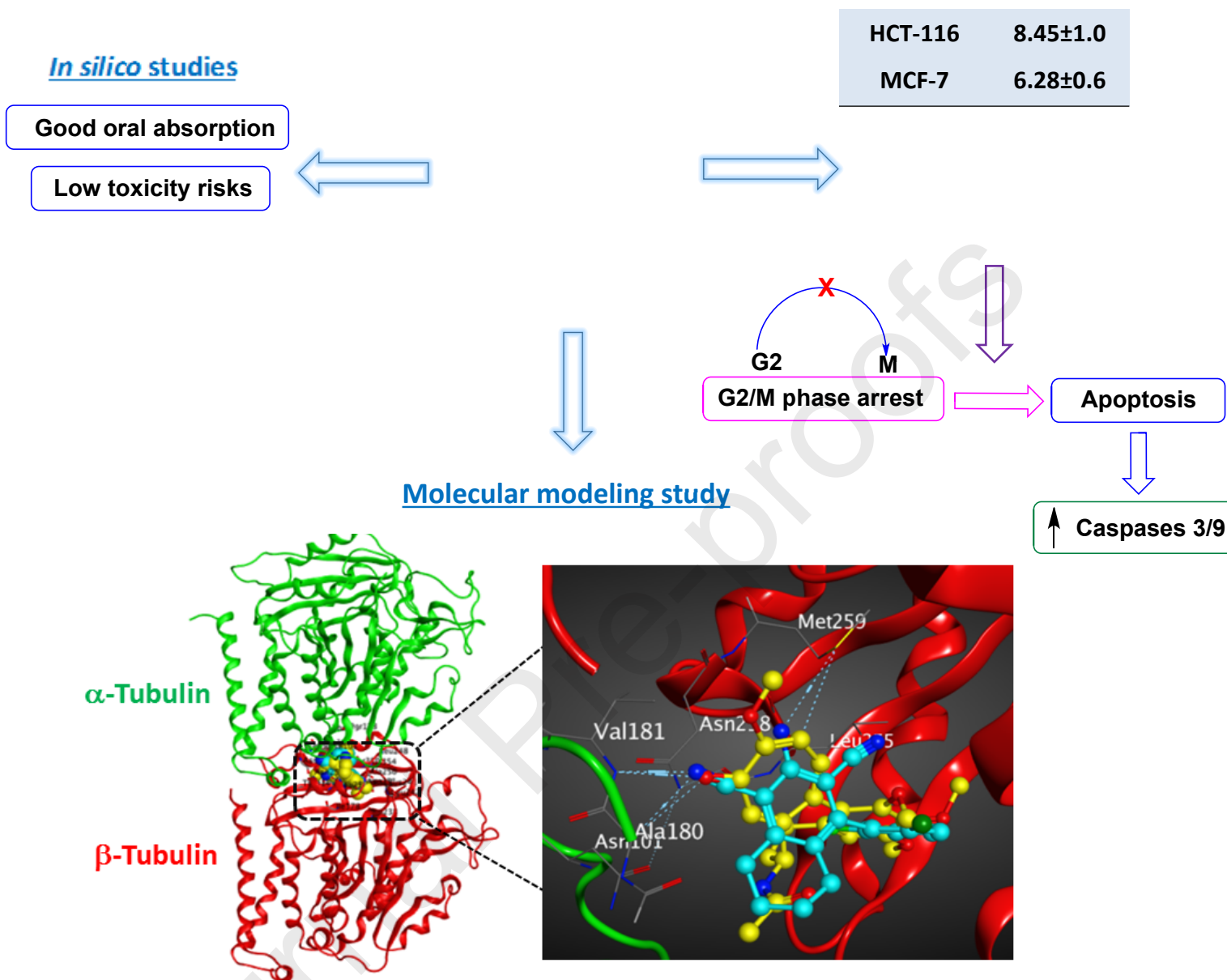
## 1,4,5,6,7,8-Hexahydroquinolines and 5,6,7,8-tetrahydronaphthalenes: A new class of antitumor agents targeting the colchicine binding site of tubulin

Mennatallah A. Shaheen, Ali A. El-Emam, Nadia S. El-Gohary

### *In vitro* antitumor testing



Cancer cell	IC <sub>50</sub> (μM)
HepG2	6.02±0.5



Compound **4c** occupied the colchicine binding site of tubulin similarly to colchicine